

## Transport of Nordic Seas overflow water into and within the Irminger Sea: An eddy-resolving simulation and observations

X. Xu,<sup>1</sup> W. J. Schmitz Jr.,<sup>2</sup> H. E. Hurlburt,<sup>3</sup> P. J. Hogan,<sup>3</sup> and E. P. Chassignet<sup>4</sup>

Received 16 April 2010; revised 16 September 2010; accepted 18 October 2010; published 18 December 2010.

[1] Results from a climatologically forced, eddy-resolving ( $1/12^\circ$ ) Atlantic simulation using the Hybrid Coordinate Ocean Model help clarify some presently unresolved connections between volume transports of Nordic Seas overflow water at key locations in the northernmost North Atlantic Ocean. The model results demonstrate that, in addition to the known westward flow through the Charlie Gibbs Fracture Zone (CGFZ), some Iceland Scotland overflow water (ISOW) flows westward through gaps in the Reykjanes Ridge north of the CGFZ into the Irminger Sea, and some flows southward along the eastern flank of the Mid-Atlantic Ridge into the West European Basin. These results provide insights into the well-known inconsistency between observed westward transport of ISOW through the CGFZ (2.4 Sv) and the transports upstream at Southeast of Iceland section (3.2 Sv) and downstream in the western Irminger Sea (4.5 Sv). Although the portion of the simulated ISOW that flows through CGFZ is about 500 m deeper than observed, the model results also show two ISOW pathways of this flow into the Irminger Sea, one northward along the western flank of the Reykjanes Ridge and the other westward before turning north-eastward on the western side of the Irminger Basin. Comparisons with the long-term moored instrument database in the Irminger Sea show that the model-based mean circulation is in reasonable agreement with observed volume transports of overflow water and that it gives approximately correct temperature and salinity characteristics.

**Citation:** Xu, X., W. J. Schmitz Jr., H. E. Hurlburt, P. J. Hogan, and E. P. Chassignet (2010), Transport of Nordic Seas overflow water into and within the Irminger Sea: An eddy-resolving simulation and observations, *J. Geophys. Res.*, 115, C12048, doi:10.1029/2010JC006351.

### 1. Introduction

[2] It has been known for some time that flow over the Greenland-Iceland-Scotland (GIS) Ridge provides regional sources of Nordic Seas overflow water (NSOW) into the northern North Atlantic Ocean [see, e.g., *Worthington and Wright*, 1970, Plate 29]. The “western source” is through the Denmark Strait [see *Ross*, 1984; *Girton et al.*, 2001, for example]. After flowing over the sill, and entraining ambient water, this bottom-trapped Denmark Strait Overflow Water (DSOW) has been observed to continue down the slope in the western Irminger Sea [e.g., *Dickson and Brown*, 1994; *Dickson et al.*, 2008; *Bacon and Saunders*, 2010]. The “eastern sources” are more complex [*Østerhus et al.*, 2008, Figure 18.1], involving bottom-

trapped flows over the Iceland-Faroe Ridge (IFR) and out through the Faroe Bank Channel (FBC). A minor contribution also spills over the Wyville-Thomson Ridge. After flowing over the IFR and the FBC sills, and entraining ambient water, the resulting Iceland-Scotland overflow water (ISOW) has been observed to flow southwestward along the northwestern slope of the Iceland Basin [*Saunders*, 1996], and westward through the Charlie-Gibbs fracture zone (CGFZ) [*Saunders*, 1994]. It has been suggested that this flow through the CGFZ subsequently turns northward into the Irminger Sea, joining DSOW there [e.g., *Dickson and Brown*, 1994; *Saunders*, 2001].

[3] DSOW and ISOW are two important components of North Atlantic Deep Water (NADW), which in addition includes Labrador Sea Water (LSW) and modified Antarctic Bottom Water (AABW). Knowledge of the circulation pathways and volume transports of these overflow water masses is therefore fundamental for a general description of the associated meridional overturning circulation in the Atlantic Ocean (often referred to as the AMOC). For related observational studies considering the source of inflow water from the North Atlantic Ocean, water transformations in the Nordic Seas, and the flow exchange over the GIS Ridge, the reader is referred to reviews by *McCartney and Mauritzen* [2001], *Mauritzen* [1996a, 1996b], *Hansen and Østerhus* [2000],

<sup>1</sup>Department of Marine Science, University of Southern Mississippi, Stennis Space Center, Mississippi, USA.

<sup>2</sup>Harte Research Institute, Texas A&M University, Corpus Christi, Texas, USA.

<sup>3</sup>Oceanography Division, Naval Research Laboratory, Stennis Space Center, Mississippi, USA.

<sup>4</sup>Center for Ocean-Atmospheric Prediction Studies, Florida State University, Tallahassee, Florida, USA.

and Hansen *et al.* [2008]. Our focus here is on the overflow water transports downstream of the GIS Ridge, but before entering the subpolar gyre.

[4] Overflow water in this area has been relatively well documented compared to further downstream. There are questions that require further clarification, however. The direct measurements of ISOW transport by Saunders [1994, 1996] lead to unresolved, although not unanticipated, questions concerning a possible branch of overflow water flowing through gaps in the Reykjanes Ridge north of the CGFZ. Questions concerning the transport of ISOW from the Iceland Basin into and within the Irminger Sea have been put forth in reviews by Saunders [2001] and Hansen and Østerhus [2000]. Specifically, (1) What is the circulation of ISOW in the Iceland Basin? (2) Does all ISOW flow westward through the CGFZ into western basins? (3) What is the flow pathway for ISOW from the CGFZ into the Irminger Sea and where (in the Irminger Sea) does it merge with DSO? Furthermore, the recent overflow transport estimates of Bacon and Saunders [2010], along with Dickson *et al.* [2008], add a new perspective to the interpretation of the basic overflow transports at key sections in the western Irminger Sea. The key interest here is to use numerical model results as an aid to observations in addressing these questions.

[5] While the spreading of overflow plumes close to the Denmark Strait or the FBC has been adequately simulated in some regional models [e.g., Shi *et al.*, 2001; Käse *et al.*, 2003; Riemenschneider and Legg, 2007], their representation in global or basin-scale models has always been a challenge. For a climate model with a horizontal resolution of  $\sim 1^\circ$ , an alternative (probably more effective) approach to explicitly simulating the overflow is to parameterize it as a marginal sea boundary condition [Legg *et al.*, 2009]. For an eddy-resolving model ( $\sim 0.1^\circ$  or finer), the main difficulty is to parameterize the entrainment process and that depends strongly on the choice of vertical coordinate [Griffies *et al.*, 2000]. A level model, by virtue of its stepped seabed, gives rise to numerically induced, unrealistic downslope spillage and consequent vertical convection, which mixes away the cold overflow water at a much too shallow depth. In contrast, an isopycnal model, in the absence of entrainment parameterization, contains insufficient diapycnal mixing and consequently the overflow properties are retained over unrealistically long distances [Willebrand *et al.*, 2001]. Transport estimates based on the long-term moored instrument arrays of Dickson and Brown [1994], Saunders [1994, 1996], Dickson *et al.* [2008], and Bacon and Saunders [2010] have formed a valuable benchmark for evaluating model performance in simulating overflow transport, which has not been well documented in the past. Some, but not all, of these transport data were used in a recent numerical study by Chang *et al.* [2009]. Their prime interest is to investigate the impact of horizontal resolution (from  $1^\circ$  to  $1/12^\circ$ ) and associated topography representation on simulating NSOW pathways. A detailed evaluation of the model-based overflow transports and water properties using the updated data is also a key interest of this investigation.

[6] The presentation is organized as follows. After this introduction, a brief summary of the key NSOW transport measurements and a description of model configurations are presented in section 2. The main results related to mean

overflow transport, as determined by a basin-scale, eddy-resolving simulation are presented in section 3, and time evolution/variation of the model solution is discussed in section 4. In section 5 the questions above are discussed within the combined framework of observations and model results.

## 2. Observations and the Ocean Model

### 2.1. A Brief Summary of Key NSOW Transport Measurements

[7] An essential component of the observational basis for overflow water in our area of interest is the volume transport estimated from five substantially instrumented, and “comparatively long” moored current meter arrays. The locations of these mooring arrays (numbered 1 through 5) are shown as sections of orange circles in Figure 1. These transport measurements are summarized in Table 1 and the reader is referred to Appendix A for a detailed account. Southeast of Cape Farewell there are also many studies considering overflow transports primarily based on hydrographic data [e.g., Bacon, 1997, 1998; Kieke and Rhein, 2006; Lherminier *et al.*, 2007; Sarafanov *et al.*, 2009; Holliday *et al.*, 2009]. Some of these studies suggest that the (baroclinic) transports of overflow water contain a significant decadal variation, which seems to be in conflict with the results based on long term moored instruments [see Dickson *et al.*, 2008, their section 19.5]. Since our interest is mainly in the mean state, we will focus the discussion on directly measured transports based on mooring arrays.

[8] The Reykjanes Ridge, which separates the Iceland Basin and the Irminger Sea, is a key topographic feature in the area of prime interest. A zoomed depiction of the bottom topography surrounding the Reykjanes Ridge is shown in Figure 2. It also depicts section 6 (denoted as a white line), across which model-determined transports through gaps in the Reykjanes Ridge are calculated (see section 3.1).

### 2.2. Model Configurations

[9] The HYbrid Coordinate Ocean model [HYCOM, Bleck, 2002; Chassignet *et al.*, 2003] is the ocean general circulation model (OGCM) used in this investigation. The vertical coordinate in HYCOM is isopycnal in the stratified open ocean and makes a dynamically smooth and time-dependent transition to terrain-following in shallow coastal regions and to fixed pressure levels in the surface mixed layer and/or unstratified seas. In doing so, the model ideally combines the advantages of the different coordinate types in optimally simulating coastal and open ocean circulation features.

[10] The primary model results for this investigation come from a basin-scale Atlantic simulation with horizontal resolution of  $1/12^\circ$  at the Equator (and about 5 km resolution in our area of interest). The computational domain extends from  $28^\circ\text{S}$  to near  $80^\circ\text{N}$  at the Fram Strait meridionally and from  $98^\circ\text{W}$  to  $36^\circ\text{E}$  zonally. The horizontal grid is a Mercator projection south of  $47^\circ\text{N}$ , and north of this latitude it uses a bipolar Arctic cap where the two poles are shifted over land to avoid a singularity at the North Pole (in a global simulation). Vertically, the simulation contains 32 hybrid layers with density referenced to 2000 m ( $\sigma_2$ ): 28.10, 28.90, 29.70, 30.50, 30.95, 31.50, 32.05, 32.60, 33.15, 33.70, 34.25,

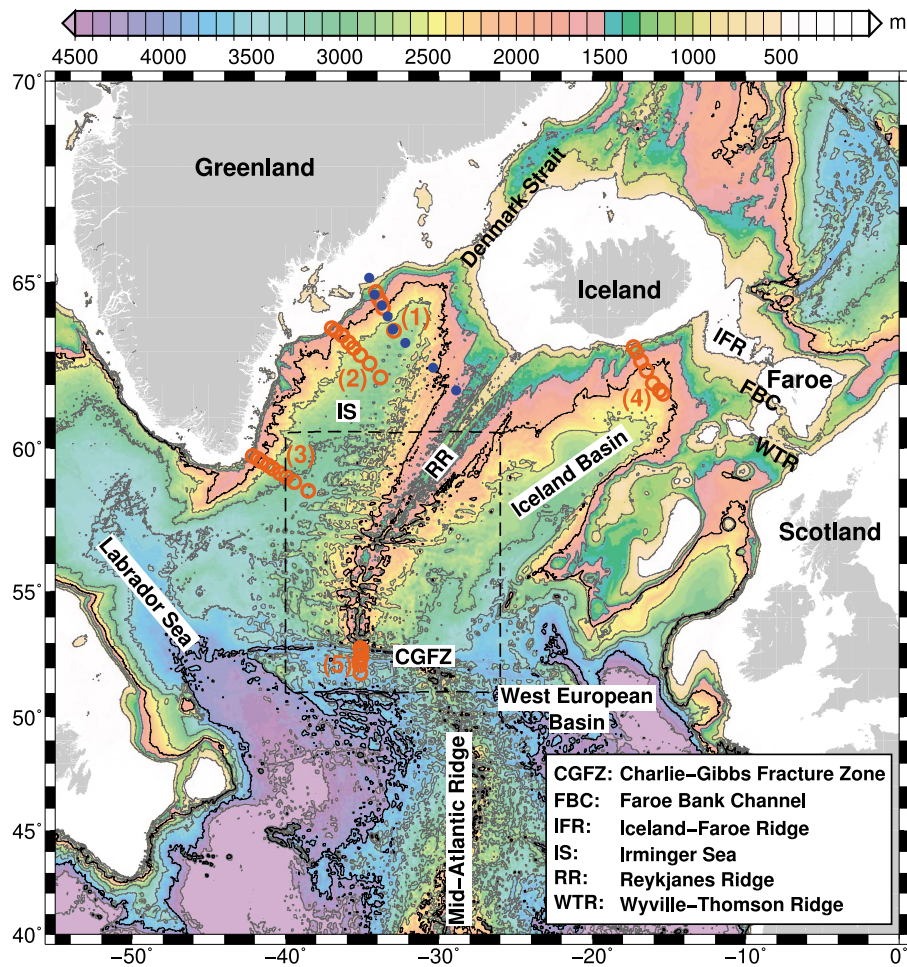


**Figure 1.** Bathymetry of the northern North Atlantic Ocean based on version 12.1 of *Smith and Sandwell* [1997]. The contour intervals are 500 m, with 2000 and 4000 m emphasized by bold black lines. Orange circles identify the locations of five long-term current meter mooring arrays that have been used to estimate the volume transports of Nordic Seas overflow water. 1, TTO [Dickson and Brown, 1994]; 2, Angmagssalik [Dickson et al., 2008]; 3, Southeast of Cape Farewell [Bacon and Saunders, 2010]; 4, Southeast of Iceland [Saunders, 1996]; 5, Charlie-Gibbs fracture zone [Saunders, 1994]. Blue dots show the locations of the hydrographic TTO section by Livingston et al. [1985]. The area outlined by the dashed black rectangle is shown in Figure 2.

34.75, 35.15, 35.50, 35.80, 36.04, 36.20, 36.38, 36.52, 36.62, 36.70, 36.77, 36.83, 36.89, 36.97, 37.02, 37.06, 37.10, 37.17, 37.30, 37.42, and 37.48 kg m<sup>-3</sup>. Layers 25–29 are connected with the overflow water. We have run sensi-

tivity experiments with more layers in the overflow water, with similar results.

[11] The model topography is based on the 2' Naval Research Laboratory (NRL) digital bathymetry database, which combines the global topography based on satellite

**Table 1.** Transports (in Sv) of Nordic Seas Overflow Water Based on Moored Current Meter Arrays at Five Locations Downstream of the GIS Ridge<sup>a</sup>

Mooring Array Number	Name	Transports	Deployment Period(s)	M/I	Key Reference
1	TTO	5.1 <sup>b</sup>	12 Jul 1990 to 30 Jul 1991	5/12	Dickson and Brown [1994]
2	ANG	7.3 <sup>b</sup> , 4.0 <sup>c</sup>	1986–1990, 1997–2005	8/24	Dickson et al. [2008]
3	SECF	9.0 <sup>b</sup> , 4.5 <sup>c</sup>	6 Sep 2005 to 30 Aug 2006	9/32	Bacon and Saunders [2010]
4	SEI	3.2 <sup>b</sup>	15 Jul 1990 to 3 Mar 1992	7/13	Saunders [1996]
5	CGFZ	2.4 <sup>b</sup>	1 Jun 1988 to 30 Sep 1989	8/16	Saunders [1994]

<sup>a</sup>TTO, Transient Tracer in the Ocean; ANG, Angmagssalik; SECF, Southeast of Cape Farewell; SEI, Southeast of Iceland; CGFZ, Charlie-Gibbs fracture zone. M/I are numbers of mooring locations and total instruments. The ANG Array includes multiple deployments with variable M/I numbers. Listed numbers are based on the most extensive deployment covering 3 July 1988 to 29 June 1989.

<sup>b</sup>The transports are evaluated for water below  $\sigma_\theta$  of 27.80 kg m<sup>-3</sup>.

<sup>c</sup>The transports are evaluated for water below  $\sigma_\theta$  of 27.85 kg m<sup>-3</sup>.

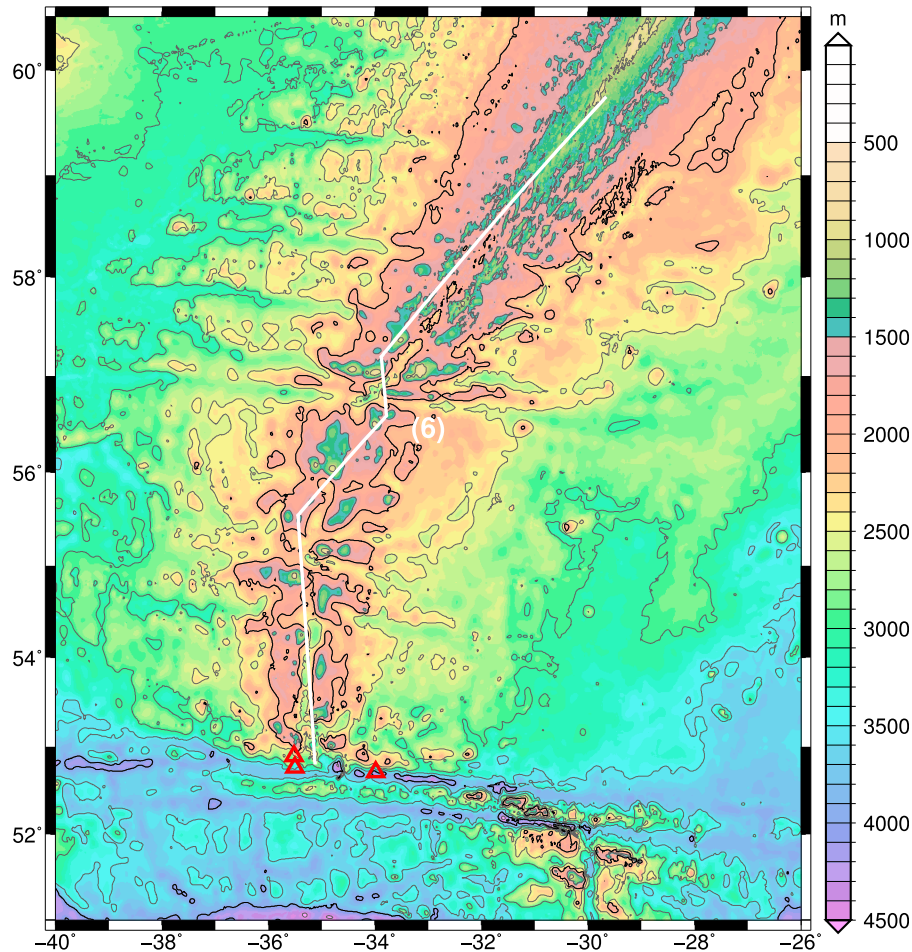


**Figure 2.** Enlargement of the area within the dashed black rectangle drawn on Figure 1. The white solid line indicates a model Reykjanes Ridge section 6, along which model-based volume transport was calculated. Red triangles show the location of three current meter moorings discussed by *Shor et al.* [1980].

altimetry of *Smith and Sandwell* [1997] with several high-resolution regional databases (see [http://www7320.nrlssc.navy.mil/DBDB2\\_WWW](http://www7320.nrlssc.navy.mil/DBDB2_WWW) for documentation). A 9-point smoother was applied once to reduce inaccurate model response at poorly resolved scales. The simulation was integrated for 20 years after initialization from rest and January temperature (T) and salinity (S) from the Generalized Digital Environmental Model (GDEM) [*Carnes*, 2009] ocean climatology. Within a buffer zone, extending about  $3^\circ$  from the northern and southern boundaries, the model T and S are restored to the same (monthly) climatology with an  $e$ -folding time scale of 5–60 days. The horizontal diffusion and viscosity parameters are listed in Table 2. For vertical/diapycnal mixing the model uses the K-profile parameterization of *Large et al.* [1994] in the surface mixed layer and in the ocean interior.

[12] The surface forcing is from a monthly climatology based on the European Center for Medium-Range Weather Forecasts reanalysis (ERA40) [*Uppala et al.*, 2005]. To better simulate the surface mixed layer, submonthly wind anomalies from the Fleet Numerical Meteorology and Oceanography Center 3 hourly  $0.5^\circ$  Navy Operational Global Atmospheric Prediction System (NOGAPS) for the year 2003 are added

to interpolated monthly means. Surface heat flux is given by

$$Q_{net} = Q_{shortwave} + Q_{longwave} + Q_{latent} + Q_{sensible}, \quad (1)$$

in which the surface short- and long-wave radiations are from ERA40, and the latent and sensible heat fluxes are calculated using the modeled sea surface temperature (SST) and the bulk formulae of *Kara et al.* [2005]. The latter provide negative feedback that increases/decreases the net

**Table 2.** Horizontal Diffusion Parameters Used in the Basin-Scale Atlantic Simulation

Diffusion Parameter	Value
Laplacian deformation-dependent viscosity coefficient	0.05
Laplacian viscosity for momentum	$20 \text{ m}^2 \text{ s}^{-1}$
Biharmonic diffusion velocity for momentum	$1.0 \text{ cm s}^{-1}$
Biharmonic diffusion velocity for layer thickness	$1.0 \text{ cm s}^{-1}$
Laplacian diffusion velocity for temperature, salinity	$0.5 \text{ cm s}^{-1}$

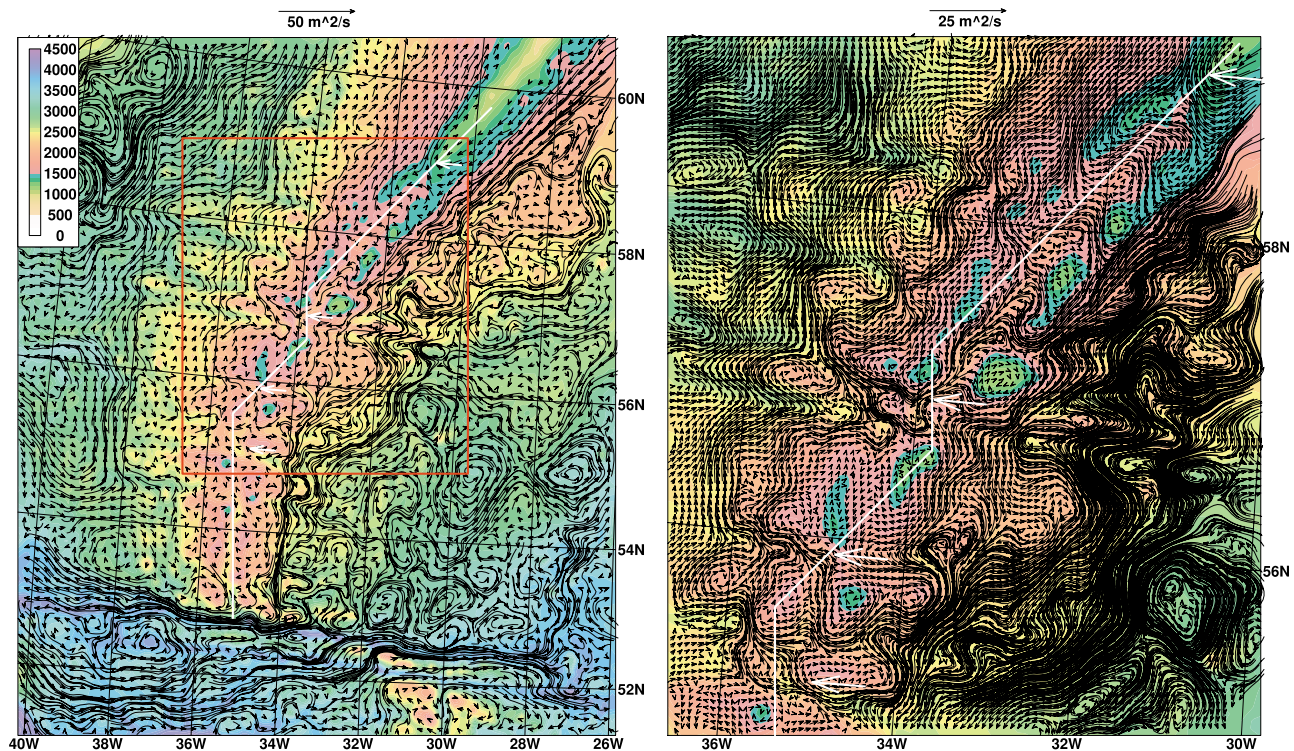


**Figure 3.** (left) Model-based mean volume transport per unit width (black arrows, in  $\text{m}^2 \text{s}^{-1}$ ) over the Reykjanes Ridge as well as through the Charlie-Gibbs fracture zone, for  $\sigma_\theta \geq 27.80 \text{ kg m}^{-3}$ . (right) Enlargement of the area marked with a orange box in Figure 3 (left). The white line denotes the model section 6, and white arrows denote the key locations where westward transport takes place.

heat flux if model SST is too cold/warm. Surface freshwater flux is treated as a virtual salinity flux,

$$F_{saln} = (E - P - R) \times SSS + V \times (S_{clim} - SSS), \quad (2)$$

in which  $E$ ,  $P$ , and  $R$  represent evaporation, precipitation, and river runoffs and the sea surface salinity ( $SSS$ ) is restored to monthly climatology with a restoring strength ( $V$ ) of 15 m/30 days. The salinity difference (between model and climatology) in  $SSS$  restoring is clipped to be 0.5 psu. The idea of reduced salinity restoring is to diminish its damping effect on ocean fronts. The reader is referred to section 3 and Appendix B of *Griffies et al.* [2009] for an insightful discussion of surface thermohaline fluxes.

### 3. Model-Based Mean Transports of NSOW

[13] We now consider model results from the eddy-resolving Atlantic simulation described in section 2.2. Specifically, how does our numerical experiment help to clarify presently unresolved connections between overflow transports, and how do model results compare to available observations? The simulation was integrated for 20 years after initialization (from climatology) and the time average of the final five years is used as the “mean” state here. We first discuss the flow over the Reykjanes Ridge north of the CGFZ in section 3.1, then follow the general spreading pathway of ISOW from the Iceland Basin, through the CGFZ, and into the Irminger Sea (3.2–3.4). The circulation in the area south of Cape Farewell is presented in section 3.5.

#### 3.1. ISOW Over the Reykjanes Ridge

[14] The observed transport through the CGFZ (2.4 Sv) based on direct measurements by *Saunders* [1994] has presented a long-standing unresolved conundrum, because it is too small to account for the ISOW found upstream and downstream [e.g., *Hansen and Østerhus* 2000]. The topic of a possible westward flow of ISOW over the Reykjanes Ridge north of the CGFZ has been mentioned by a few authors (see section A2). Here we use results based on an eddy-resolving numerical experiment, with about 5 km resolution around  $57^\circ\text{N}$ , and model-data comparisons to demonstrate the likelihood that some ISOW flows into the Irminger Sea through gaps in the Reykjanes Ridge.

[15] The model-based mean circulation of ISOW surrounding the Reykjanes Ridge and the CGFZ area is illustrated in Figure 3. As has long been realized, the CGFZ is the principle conduit carrying ISOW from the Iceland Basin to the western side of the Mid-Atlantic Ridge (MAR). It is not the sole conduit, however. As shown in the zoomed Figure 3 (right), some model-based ISOW flows into the Irminger Sea over the shallow Reykjanes Ridge near  $59^\circ\text{N}$ , some through the relatively deep Bight Fracture Zone near  $57^\circ\text{N}$ , and some through a couple of unnamed gaps/valleys between  $55^\circ\text{N}$  and  $56^\circ\text{N}$ . Along section 6 over the Reykjanes Ridge (denoted as the white line in Figure 3), the model-based mean normal velocity and the accumulated volume transports are displayed in Figure 4. The mean velocity of ISOW over the Ridge is about  $1\text{--}2 \text{ cm s}^{-1}$  westward. The model-

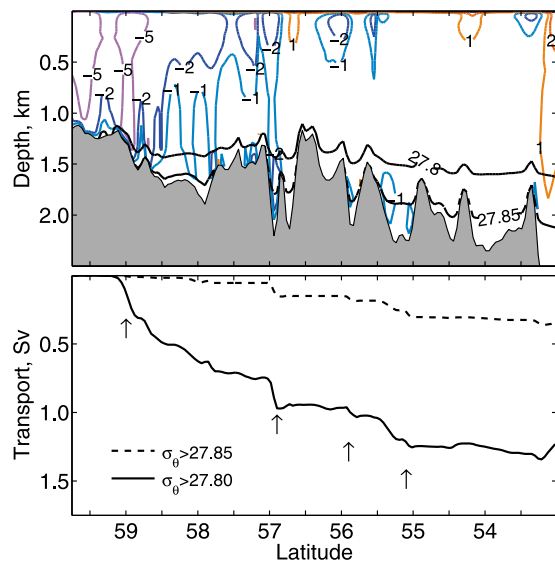


**Figure 4.** (top) Model-based mean normal velocity ( $\text{cm s}^{-1}$ ) and (bottom) accumulated volume transports (Sv) along model section 6 that follows the Reykjanes Ridge crest. Upward arrows in Figure 4 (bottom) denote four latitudes at which key westward transport takes place along the section.

determined mean transport for water below  $27.80 \text{ kg m}^{-3}$  is  $1.2 \text{ Sv}$ , half of the value observed through the CGFZ.

[16] To further demonstrate that a westward flow of ISOW over the Reykjanes Ridge is possible, we have plotted the salinity distribution based on historical bottle data collected in the World Ocean Database (Figure 5). The high salinity water sitting over the Reykjanes Ridge south of about  $58^\circ\text{N}$ , with density greater than  $27.80 \text{ kg m}^{-3}$ , is a clear signature of ISOW. The highest salinity of ISOW is found in the Bight Fracture Zone near  $57^\circ\text{N}$ . For comparison, the model-based salinity distribution is also shown in Figure 5. There are differences. For example, the observations show a subsurface low salinity core associated with LSW in the CGFZ, while it is found over the Reykjanes Ridge in model. Nevertheless, the overall structure and the saline ISOW over the Reykjanes Ridge roughly agrees with observations.

### 3.2. ISOW in the Iceland Basin

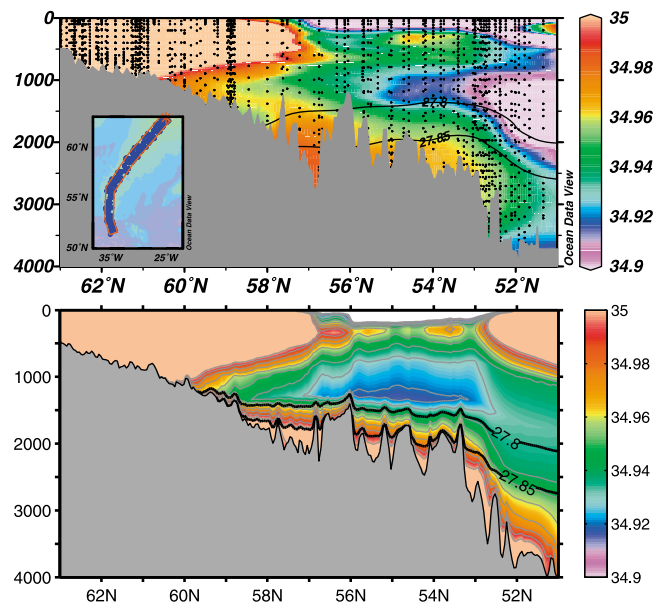
[17] Along a section collocated with the mooring array deployed southeast of Iceland (SEI hereafter), the model-based vertical distribution of mean salinity, mean normal velocity, and the accumulated volume transport are illustrated in Figure 6a. Here the simulated ISOW is seen as a bottom trapped layer of saline water on the Icelandic slope, occupying a depth range from  $1300 \text{ m}$  to the maximum depth of this section (about  $2300 \text{ m}$ ). The maximum ISOW salinity is about  $35.04 \text{ psu}$ . Relatively fresh LSW with a salinity minimum of about  $34.94 \text{ psu}$  is centered at a depth of  $1600 \text{ m}$  in the middle of the Iceland Basin. The warm and saline MNAW ( $7^\circ\text{C}$ – $8^\circ\text{C}$  and  $35.1$ – $35.3 \text{ psu}$ ) occupies the upper  $600$ – $1000 \text{ m}$  above the halocline (also the thermocline). While the maximum salinity of modeled MNAW is about  $0.1 \text{ psu}$  higher than observed, this three-layer salinity structure agrees well with observations [see Saunders, 1996,

Figure 2b]. Strong currents are simulated within the ISOW on the mid Icelandic slope ( $20$ – $25 \text{ cm s}^{-1}$  near the  $1500 \text{ m}$  contour) and decrease toward the deeper part of the section ( $2$ – $5 \text{ cm s}^{-1}$  at depths greater than  $2000 \text{ m}$ ). This simulated horizontal pattern and flow magnitude roughly agrees with observations [see Saunders, 1996, Table 2 and Figure 4]. The model-based accumulated volume transport has a maximum of  $3.3 \text{ Sv}$  for  $\sigma_\theta \geq 27.80 \text{ kg m}^{-3}$ . A transport of  $3.2 \text{ Sv}$  was observed by Saunders [1996].

[18] Spreading of the modeled deep ISOW in the Iceland Basin, as defined by volume transport per unit width (in  $\text{m}^2 \text{ s}^{-1}$ ) below  $\sigma_\theta$  of  $27.85 \text{ kg m}^{-3}$ , is displayed in Figure 7. Southwest of Iceland, the modeled ISOW separates into three main branches. The westernmost (shallowest) branch flows parallel to the Reykjanes Ridge and contributes to the flow across the Reykjanes Ridge north of the CGFZ (also see Figure 3). The middle branch follows along a depth contour of about  $2500 \text{ m}$  and contributes mainly to the flow through the CGFZ. The deepest branch flows into the deepest part of the Iceland Basin and does not contribute to the westward flow. These branches of the ISOW plume closely follow contours of the bottom topography in the Iceland Basin. Superimposed on Figure 7 are the crests of three depositional drifts reproduced from Figure 5.6.4 of Saunders [2001]. These sedimentation patterns, called the Björn, Björnsson, and Gardar Drifts, are thought to be formed by the interaction of ISOW with sediment in the Iceland Basin (for more detail see Bianchi and McCave [2000]).

### 3.3. Flow Through the Charlie-Gibbs Fracture Zone

[19] Figure 6b depicts the model-based vertical distribution of the mean salinity and normal velocity along the



**Figure 5.** Vertical distribution of salinity (in psu) along the Reykjanes Ridge and across the Charlie-Gibbs fracture zone based on (top) observations and (bottom) the model. The observations are from the historical ocean station data collected in the World Ocean Database 2005 (WOD05, <http://www.nodc.noaa.gov>). The insert map illustrates the location of selected stations.

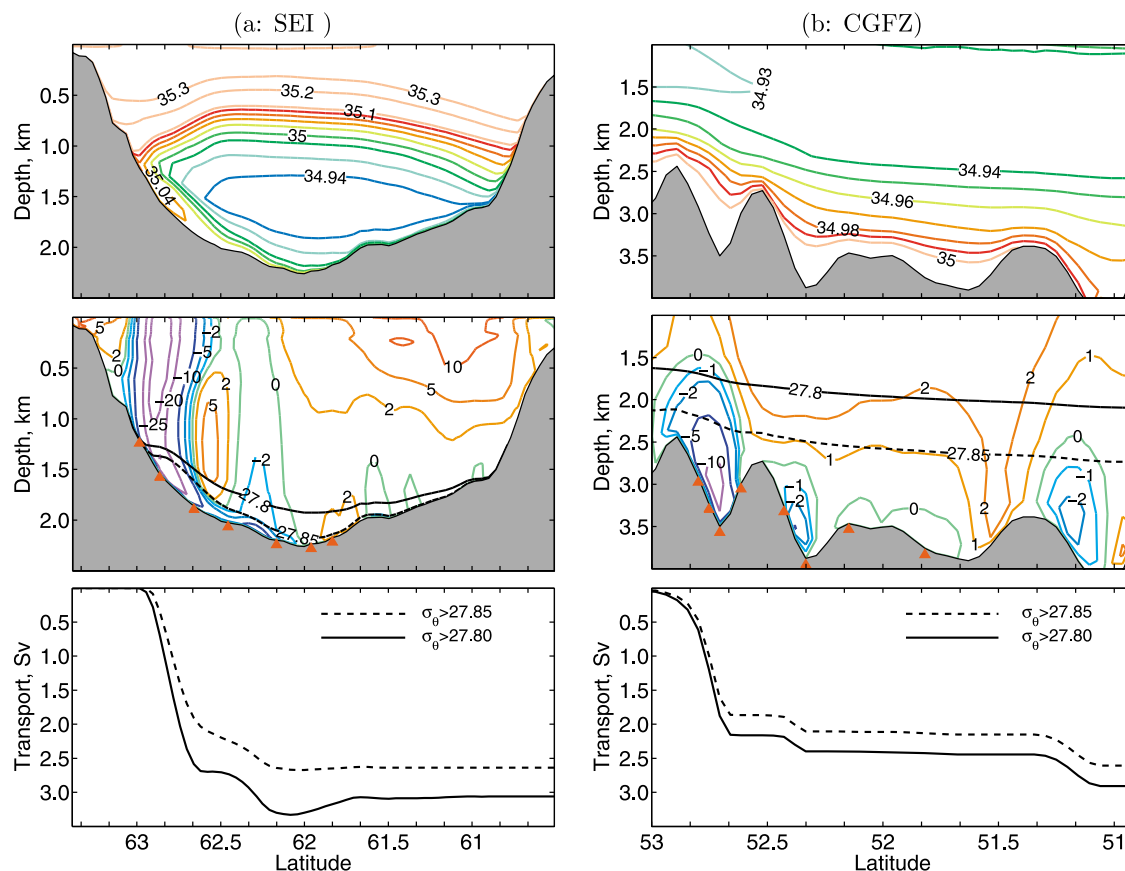


**Figure 6.** (top) Model-based mean salinity (psu), (middle) normal velocity ( $\text{cm s}^{-1}$ ), and (bottom) accumulated volume transports (Sv) along two mooring arrays in the Iceland Basin: (a) Southeast of Iceland and (b) Charlie-Gibbs fracture zone along  $35^\circ\text{W}$ . The orange triangles mark the approximate mooring locations. Note transports through the CGFZ are for westward flow only.

CGFZ array near longitude  $35^\circ\text{W}$ . The northern channel of the CGFZ in the model has a sill depth of 3428 m, compared to 3675 m observed [Shor *et al.*, 1980]. The simulated ISOW has a maximum salinity of about 35.0 psu close to the bottom. This is slightly more saline than observed [see Saunders, 1994, Figure 2] and the depth of the salinity maximum is also about 500 m deeper. The modeled isopycnal  $27.80 \text{ kg m}^{-3}$  gradually deepens from about 1500 m at  $53^\circ\text{N}$  to 2000 m at  $51.5^\circ\text{N}$  in agreement with observations. The model-determined westward flow (Figure 6b) is stronger in the northern channel (about  $10 \text{ cm s}^{-1}$ ) than in the southern channel ( $2\text{--}5 \text{ cm s}^{-1}$ ). This flow distribution and magnitude compare quite well with observations [see Saunders, 1994, Table 3 and Figure 6]. Within the area of mooring coverage, the accumulated volume transports of the simulated westward flow are 2.4 and 2.1 Sv, for water below  $\sigma_\theta$  of 27.80 and 27.85  $\text{kg m}^{-3}$ , respectively (Figure 6b, bottom).

[20] Figure 8 illustrates the mean circulation of model-based deep ISOW ( $\sigma_\theta \geq 27.85 \text{ kg m}^{-3}$ ) in the vicinity of the CGFZ. The net southward transport of the modeled deep ISOW is 2.5 Sv across the southern Iceland Basin near  $54^\circ\text{N}$  (not shown). About 1.9 Sv of this deep ISOW flows through various gaps west of  $32^\circ\text{W}$  and turns westward in the northern channel of the CGFZ. The rest, which flows southward east of  $32^\circ\text{W}$ , turns eastward in the eastern part

of northern channel. This eastward flow is found above the sill of the northern channel and therefore is unlikely a result of topographic blocking. The model-based flow in the southern channel of the CGFZ is also westward and contains a high-salinity signature similar to that in the northern channel (see Figure 6b). Figure 8, however, suggests that this westward flow is not fed from the Iceland Basin, but rather is a localized recirculation feature. Also, the small westward transport (0.3 Sv) between 27.80 and 27.85  $\text{kg m}^{-3}$  is fed from an eastward flow in the southern part of the CGFZ. Therefore, the model-determined “net” transport of ISOW from the Iceland Basin through CGFZ is 1.9 Sv westward with  $\sigma_\theta$  larger than 27.85  $\text{kg m}^{-3}$ . This is 0.5 Sv less than the 2.4 Sv based on data [Saunders, 1994].

[21] The model results also show eastward flows that extends below  $\sigma_\theta$  of 27.80  $\text{kg m}^{-3}$  south of about  $52.5^\circ\text{N}$  and all the way to the bottom near  $51.5^\circ\text{N}$  (Figure 6b). Below 27.85  $\text{kg m}^{-3}$ , the eastward flow eventually feeds into the northern channel of the CGFZ through several gaps around  $32^\circ\text{W}$  and merges with the eastward flow contributed from the Iceland Basin. East of about  $28^\circ\text{W}$  the combined eastward flow (about 1 Sv) turns southward and flows along the eastern flank the MAR. If this southward flow is realistic, it would account for the ISOW tracer signals observed in the West European Basin (WEB) by Fleischmann and Rhein [2000] and Fleischmann *et al.* [2001]; see also

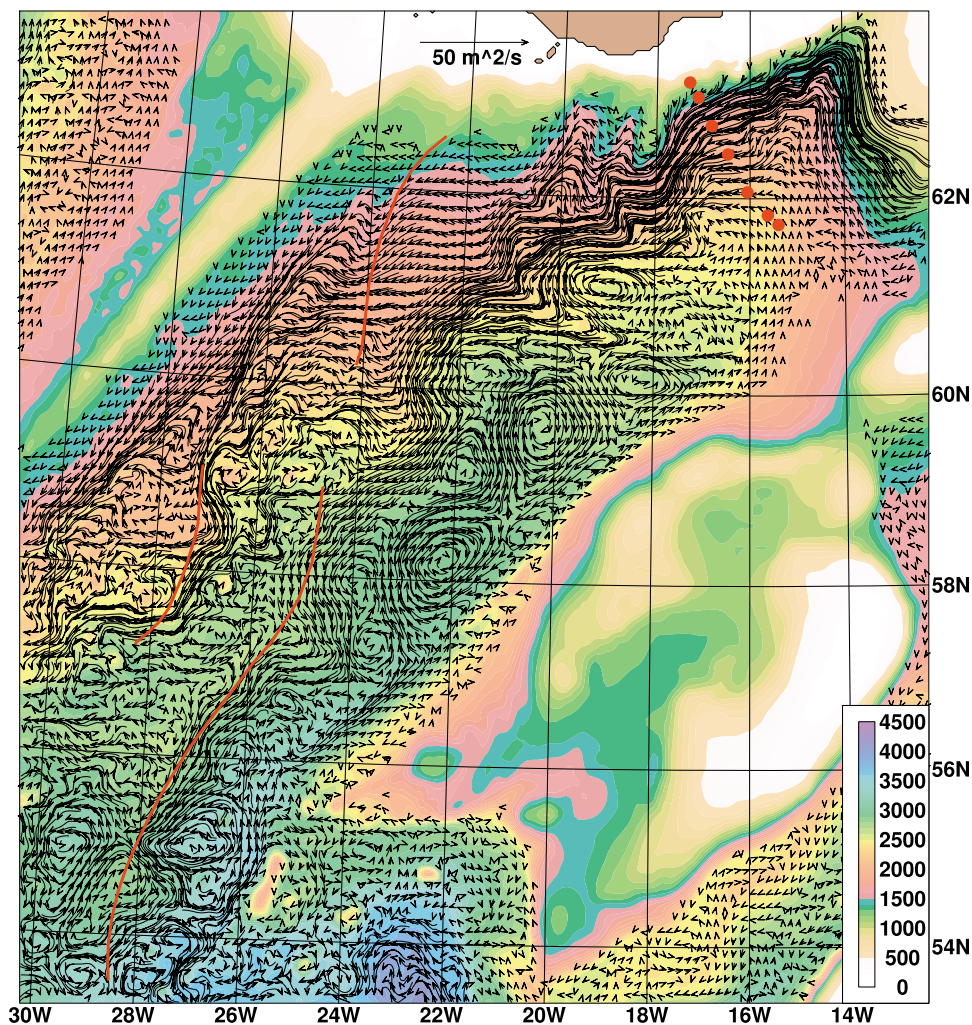


**Figure 7.** Model-based mean vectors of volume transport (per unit width, in  $\text{m}^2 \text{s}^{-1}$ ) for  $\sigma_\theta \geq 27.85 \text{ kg m}^{-3}$  in the Iceland Basin. The orange lines, taken from Figure 5.6.4 of *Saunders* [2001], represent the crests of three sedimentary drifts formed by persistent bottom currents.

*Hansen and Østerhus* [2000, Figure 54] and *Saunders* [2001]. Based on the observed tracer signals, *Fleischmann et al.* [2001] estimated a southward transport of 2.4–3.5 Sv (corresponding to  $\sigma_\theta \geq 27.80 \text{ kg m}^{-3}$ ) from the Iceland Basin into the WEB. The model results yield a net southward transport of 2.6 Sv into the WEB. About 2 Sv are from west of the CGFZ and most of it has  $\sigma_\theta < 27.85 \text{ kg m}^{-3}$ . It seems possible that via recirculations and mixing, the eastward flow through the CGFZ is tagged with the tracer signals of ISOW. We also note that in addition some eastward flow with  $\sigma_\theta$  between 27.80 and 27.85  $\text{kg m}^{-3}$  flows northward into the Iceland Basin and adds to the ISOW transport over the Reykjanes Ridge.

### 3.4. Circulation Within the Irminger Sea

[22] For simplicity, we use the location of the Southeast of Cape Farewell (SECF hereafter) mooring array as a southern boundary of the Irminger Sea. The model-determined mean circulation in the Irminger Sea is shown for two layers in Figure 9. For  $\sigma_\theta \geq 27.85 \text{ kg m}^{-3}$  (Figure 9a), the circulation is dominated by the southward flowing DSOW along the

western boundary. The flow of deep ISOW into and in the Irminger Sea roughly follows the deepest trough of the basin. For  $27.80 \leq \sigma_\theta < 27.85 \text{ kg m}^{-3}$  (Figure 9b), this upper overflow layer circulation is generally cyclonic around the basin and contains inputs from the Denmark Strait, from east of the Reykjanes Ridge, as well as from recirculation south of Cape Farewell. To shed some light on the location(s) where ISOW joins DSOW, we draw a straight white line in Figure 9 from the Denmark Strait southwestward along the Irminger Sea trough roughly in parallel with the Reykjanes Ridge. The accumulated volume transports along this line are shown in Figure 10. The model results suggest that the crossing (from east to west) is approximately evenly distributed for  $\sigma_\theta \geq 27.85 \text{ kg m}^{-3}$ . In contrast, significantly more crossing takes place north of the ANG line for  $27.80 \leq \sigma_\theta < 27.85 \text{ kg m}^{-3}$ . One reason is that the less dense ISOW through the gaps in the Reykjanes Ridge flows around the northern end of the Irminger Sea.

[23] The distributions of mean salinity and velocity across the basin are shown in Figure 11 along model sections that are collocated with the ANG and SECF arrays. The model-

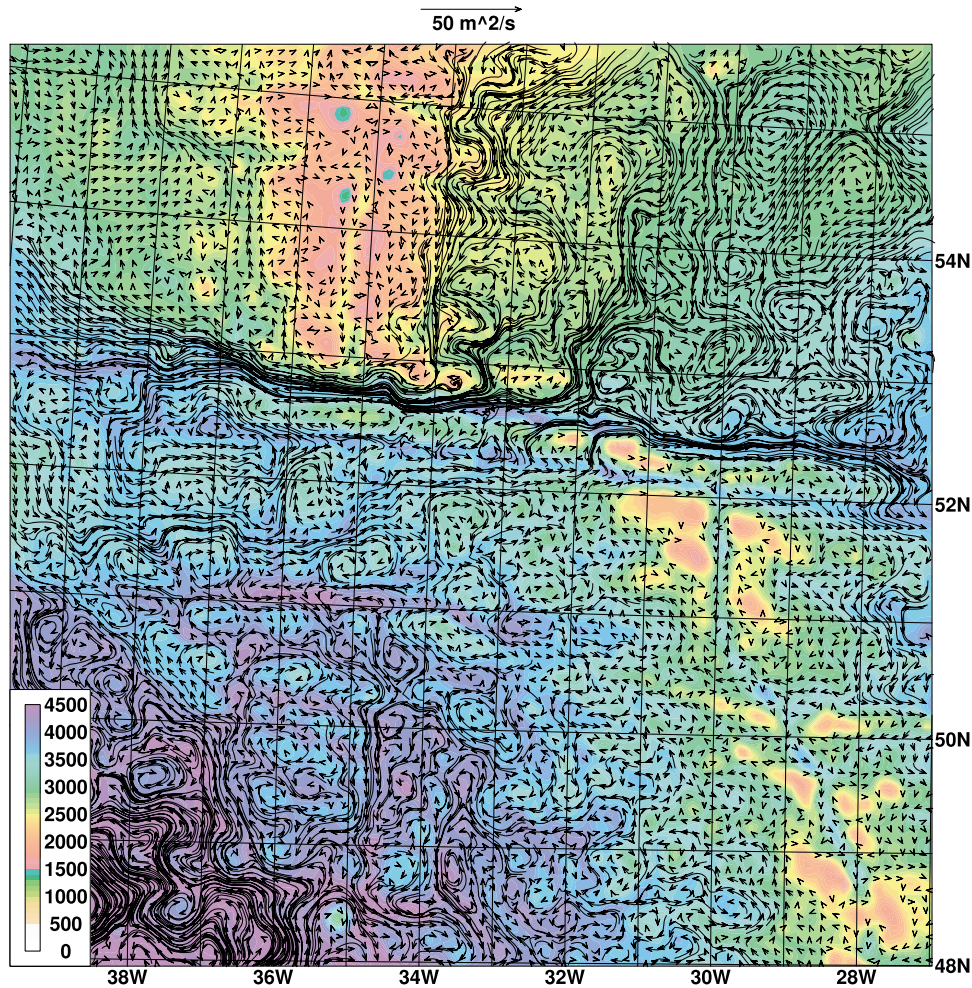


**Figure 8.** Model-based mean vectors of volume transport (per unit width, in  $\text{m}^2 \text{s}^{-1}$ ) for  $\sigma_\theta \geq 27.85 \text{ kg m}^{-3}$  in a region centered on the Charlie-Gibbs fracture zone.

based salinity contains a structure similar to that observed in the Irminger Sea (see Figure A1 in section A3, for an example). The model flows are generally strong and south-westward along the western boundary, weak and northeastward through the eastern half of the sections. Within the western boundary region, the current speeds decrease from the (shallow) continental slope toward the deeper part of the sections. The easternmost mooring of both arrays shows northward flow, see Figure 12 of *Dickson and Brown* [1994] for the ANG array [see also *Saunders*, 2001, Figure 5.6.5] and Figure 11 of *Bacon and Saunders* [2010] for the SECF array. The reversal in flow direction marks the eastern edge of the western boundary current, and the simulated flow reversal along these two arrays agrees well with observations (see Figure 9). Vertically, the moorings of these two arrays contain multiple instruments (up to six in the ANG array), and therefore to some extent resolve the vertical structure of the velocity within the overflow layer. A direct comparison of the velocity profiles is presented in Figure 12 for both arrays. The model-based profiles reproduce to some degree the observed bottom intensification of the mean speed at the deep mooring locations, but not at shallow stations.

[24] Along the western boundary at the ANG section, the model-determined volume transports are 7.8 and 4.6 Sv for  $\sigma_\theta \geq 27.80$  and  $27.85 \text{ kg m}^{-3}$ , compared to 7.3 and 4 Sv based on observations [*Dickson et al.*, 2008, Table 19.2]. At the SECF section, these two values are 9.4 and 5.6 Sv from the model results, in comparison to 9.0 and 4.5 Sv based on data [*Bacon and Saunders*, 2010]. At this point, we summarize the model-determined circulation in terms of a transport budget. The transport of DSOW into the Irminger Sea through the Denmark Strait Sea is 3.2 Sv for  $\sigma_\theta \geq 27.80 \text{ kg m}^{-3}$  and 2.9 Sv for  $\sigma_\theta \geq 27.85 \text{ kg m}^{-3}$ . Downstream about halfway through the basin at the ANG section, the “net” transports across the entire Irminger Sea increase to 4.0 and 3.4 Sv for water below 27.80 and  $27.85 \text{ kg m}^{-3}$ , respectively. This increase is due to the entrainment of ambient water. Focusing on the SECF section, the model-determined western boundary transport of 9.4 Sv for  $\sigma_\theta \geq 27.80 \text{ kg m}^{-3}$  includes about 4.0 Sv DSOW and 3.1 Sv ISOW that flows through gaps in the Reykjanes Ridge and through the northern channel of the CGFZ. The remainder is due to recirculation (about 2.3 Sv, discussed below). For  $\sigma_\theta \geq 27.85 \text{ kg m}^{-3}$ , the model-determined boundary transport of 5.6 Sv is the sum of 3.4 Sv DSOW and 2.2 Sv ISOW that flows over the Reykjanes Ridge and through the northern channel of the CGFZ.

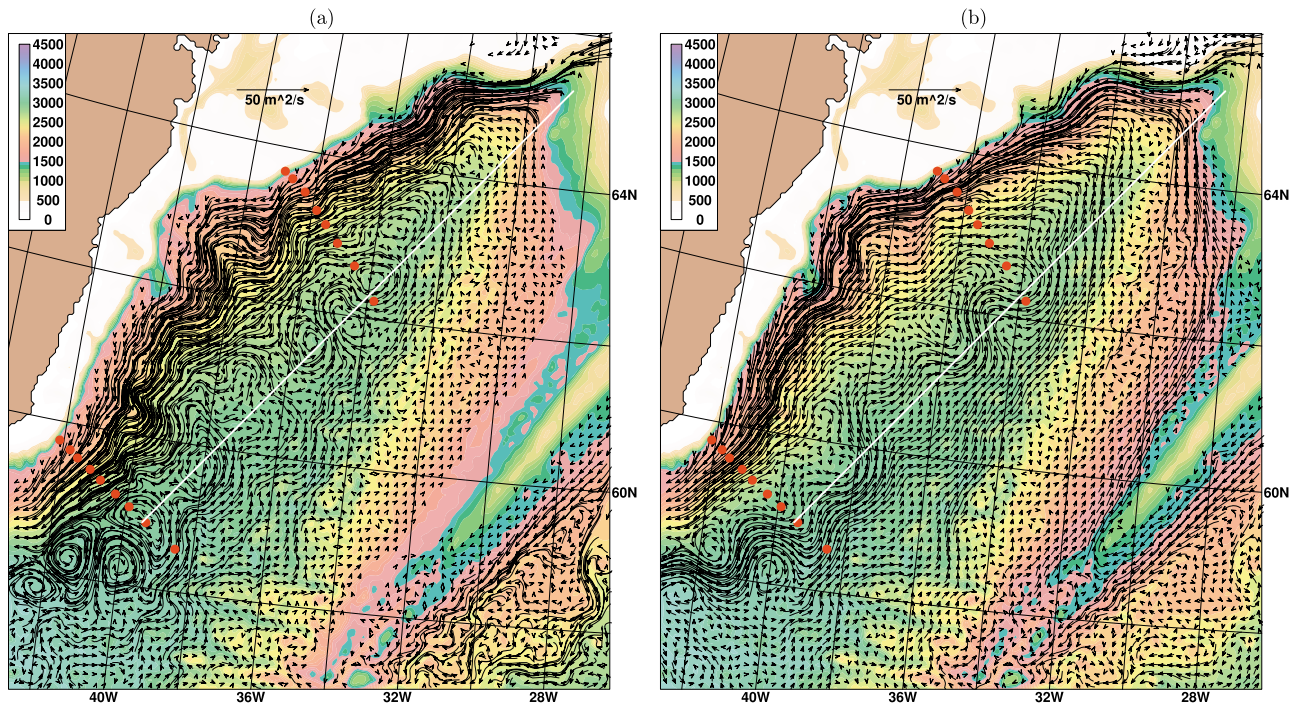


**Figure 9.** Model-based mean vectors of volume transport (per unit width,  $m^2 s^{-1}$ ) in the Irminger Sea for (a)  $\sigma_\theta \geq 27.85 \text{ kg m}^{-3}$  and (b)  $27.80 \leq \sigma_\theta < 27.85 \text{ kg m}^{-3}$ . The white line denotes a section along which model-based volume transport was calculated. Orange dots denote the location of two mooring arrays (2 and 3 shown in Figure 1).

### 3.5. Flow West of the CGFZ and South of Cape Farewell

[25] West of the CGFZ, the ISOW (that has passed through the CGFZ) is generally assumed to flow northward into the eastern side of the Irminger Sea, eventually turning westward and merging with/overriding the DSOW flowing southwestward. But details of the spreading pathway(s) remain unanswered. The model-based mean circulation of deep ISOW in the area between the CGFZ and SECF mooring arrays is displayed in Figure 13a. In the longitude range 36–39°W, part of the westward flowing deep ISOW splits off to form a northward branch along the western flank of the Reykjanes Ridge. This flow merges with westward currents through gaps in the Reykjanes Ridge and penetrates into the northern Irminger Sea. The rest of the deep ISOW, however, follows a deeper and more western route, and after passing a complex topographic feature around 45°W, 56°N (called Gloria Drift), eventually reaches the area south of Cape Farewell. There the southwestward flowing Deep Western Boundary Current (DWBC) and the northeastward flowing ISOW are nearly adjacent. Several closed cyclonic and anticyclonic recirculations are formed, and mixing between two water masses is to be expected. A small portion of the deep ISOW may join the southwest flow of DWBC into the Labrador Sea, while the rest continues to flow eastward to northeastward into the Irminger Sea.

[26] The model results also depict a large scale cyclonic recirculation west of the northwestward deep ISOW flow in the Labrador Sea and east of the southeastward DWBC along the Labrador coast. Below  $\sigma_\theta$  of  $27.85 \text{ kg m}^{-3}$  (Figure 13a), the recirculation occupies the deepest area (>3500 m) from

51 to 58°N mostly within the Labrador Sea. In the overflow layer between  $\sigma_\theta$  of 27.80 and 27.85  $\text{kg m}^{-3}$  (Figure 13b), the recirculation includes a well-defined eastward to northeastward “jet” south of Cape Farewell penetrating into the Irminger Sea. Transport of this jet is about 2.2 Sv, consistent with the transport balance discussed in section 3.4. This recirculation component, if realistic, raises a question regard-

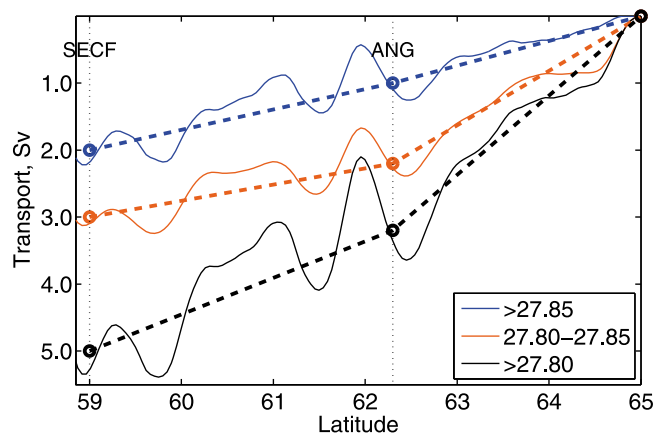


**Figure 10.** Model-based accumulated volume transports (in Sv) across the white line in Figure 9. Black dotted lines denote the approximate location of two mooring arrays: Angmagssalik (ANG) and Southeast of Cape Farewell (SECF). Thick dashed lines are linear approximations of the transport accumulation north and south of the ANG Array.

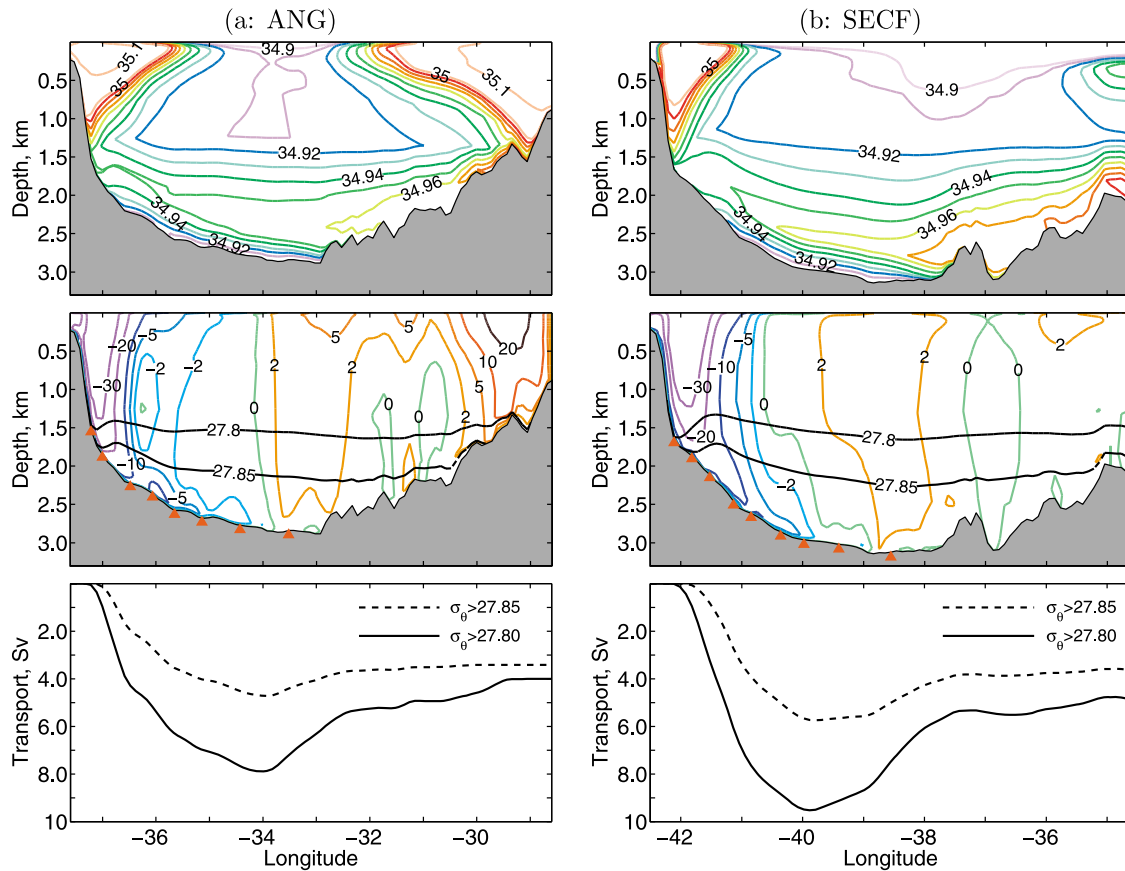


**Figure 11.** (top) Model mean salinity (psu), (middle) normal velocity ( $\text{cm s}^{-1}$ ), and (bottom) accumulated volume transports (Sv) along two mooring arrays in the Irminger Sea: (a) Angmagssalik and (b) Southeast of Cape Farewell. Orange triangles mark the approximate mooring locations.

ing the source of the volume transports that have been estimated along the western Irminger Sea. *Dickson et al.* [2008, p. 462] mentioned that the transports of DSO (based on hydrography) appear to increase downstream from sections south of the ANG array to southeast of Cape Farewell and suggested that this increase might be due to a recirculation loop within the Irminger Sea. We should also note that in this area recirculation is a commonly observed above the overflow water in the regime of LSW [e.g., *Lavender et al.*, 2000, 2005; *Faure and Speer*, 2005]. The model results suggest recirculations may exist deep in the overflow water as well.

#### 4. Temporal Variation of the Model-Based NSOW

[27] We now shift our focus from long-time averages to temporal variation of the model results. A 20 year integration of the simulation is relatively short in terms of reaching a model equilibrium, especially for water properties. This warrants some documentation of how the model-based NSOW evolves over the integration period. Besides, the observed transports typically are based on moored instrument records of about 1 year. It is therefore useful to examine if the model results contain nondeterministic, long-term variations that are not due to external forcing.

#### 4.1. Overflow Sources at the Denmark Strait and Through the FBC

[28] Figure 14 shows the model-based volume transport and average temperature ( $\bar{T}$ ) and salinity ( $\bar{S}$ ) of the overflow source water at the Denmark Strait and out through the FBC, plotted as a function of time. Both  $\bar{T}$  and  $\bar{S}$  are transport weighted, using

$$\bar{T} = \frac{\int_0^L \int_{z_l}^{z_u} T v dz dx}{\int_0^L \int_{z_l}^{z_u} v dz dx}, \quad (3)$$

$$\bar{S} = \frac{\int_0^L \int_{z_l}^{z_u} S v dz dx}{\int_0^L \int_{z_l}^{z_u} v dz dx}. \quad (4)$$

The denominator in above equations denotes the volume transport, in which  $v$ ,  $L$ ,  $z_u$ , and  $z_l$  represent the normal velocity, the horizontal span, the upper, and lower interfaces of the overflow water. Transport and water properties of DSO at or near the Denmark Strait sill have been topics of many studies [see *Ross*, 1984; *Dickson and Brown*, 1994; *Rudels et al.*, 1999; *Girton et al.*, 2001; *Macrandar et al.*, 2005]. A transport value of about 3 Sv, with  $\bar{T}$  of 0–1.2°C and  $\bar{S}$  of slightly less than 34.90 psu is a typical estimate. After about 5 years of integration, the simulated DSO at the Denmark Strait reached an equilibrium state, with a

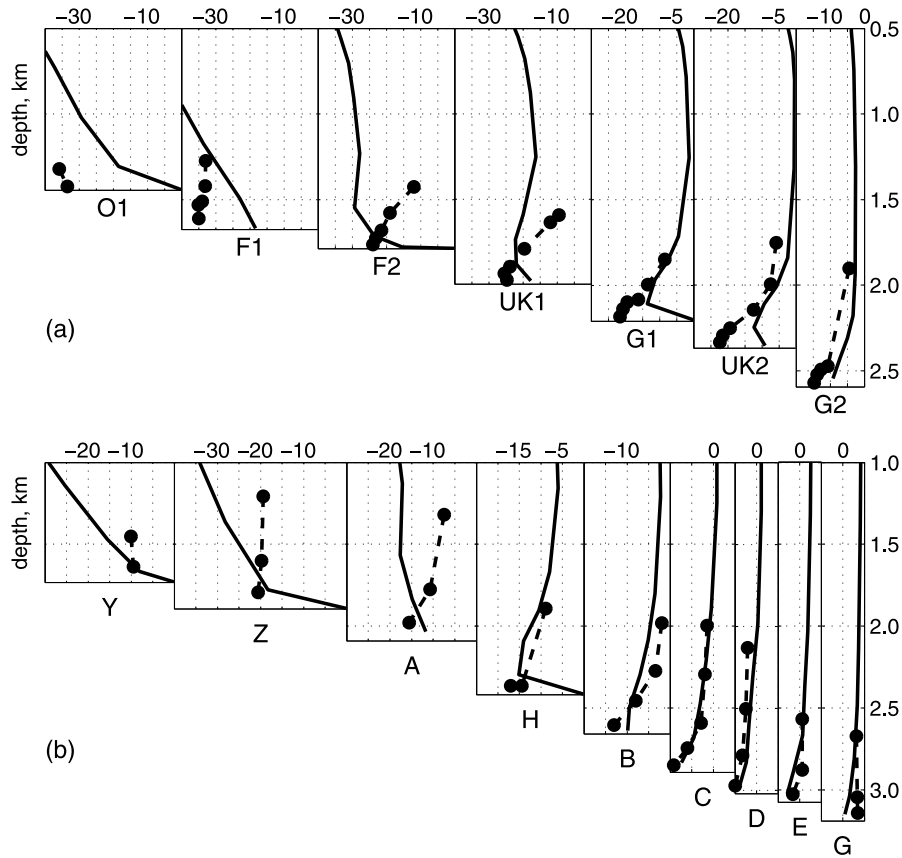


**Figure 12.** Comparison of simulated mean along slope velocities (solid line) with data from two mooring arrays in the western Irminger Sea: (a) Angmagssalik, data from Figure 19.6 of *Dickson et al.* [2008] and (b) Southeast of Cape Farewell, data from Table 2 of *Bacon and Saunders* [2010].

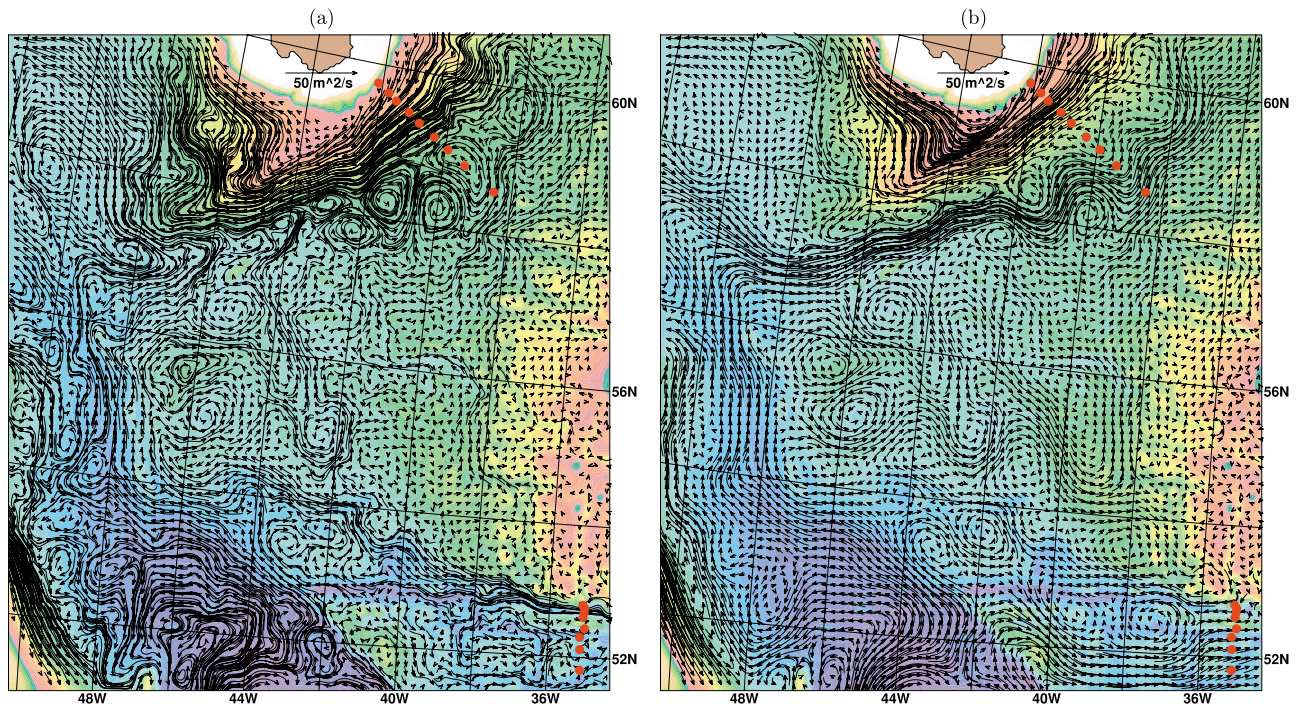


**Figure 13.** Model-based mean vectors of volume transport (per unit width,  $\text{m}^2 \text{s}^{-1}$ ) in the area south of Cape Farewell and west of the Charlie-Gibbs fracture zone for (a)  $\sigma_\theta \geq 27.85 \text{ kg m}^{-3}$  and (b)  $27.80 \leq \sigma_\theta < 27.85 \text{ kg m}^{-3}$ .

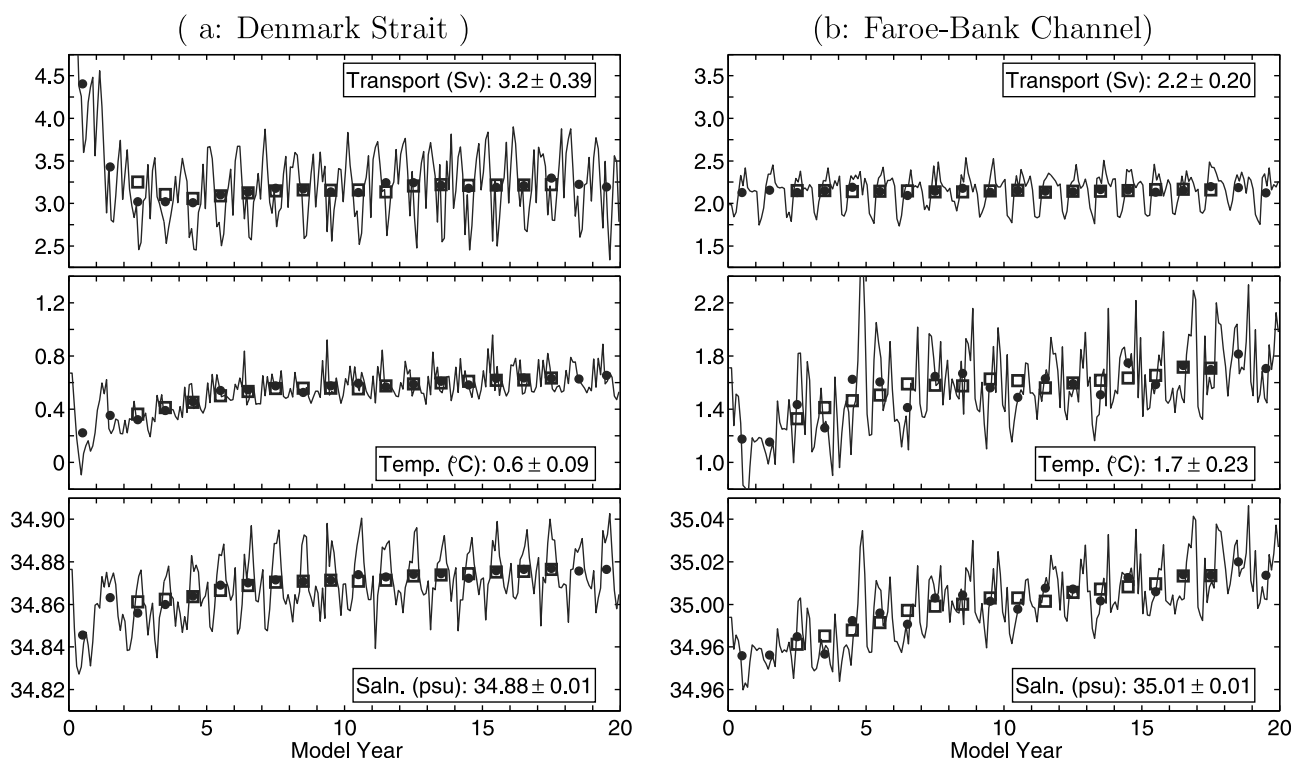


**Figure 14.** Time evolution of the model-based volume transport, averaged  $T$  and  $S$  of DSOW and ISOW at sills of (a) the Denmark Strait and (b) the Faroe Bank Channel. Lines, dots, and squares are results based on monthly means, annual means, and 5 year means, respectively.

transport of  $3.2 \pm 0.4$  Sv,  $\bar{T}$  of  $0.6 \pm 0.1$  °C, and  $\bar{S}$  of  $34.88 \pm 0.01$  psu. The standard deviation values are based on the monthly means of the final 5 years of integration. Overall, the model-based DSOW at the Denmark Strait agrees well with observations. The modeled transport contains a seasonal cycle that is not a characteristic of observations.

[29] The overflow water out through the FBC has been well-quantified based on long-term, moored instrument data [see Hansen and Østerhus, 2007]. It has a volume transport of  $1.9 \pm 0.3$  Sv, with  $\bar{T}$  and  $\bar{S}$  of  $0.25$  °C and  $34.93$  psu, respectively. The observed transport contains a seasonal variation which accounts for about 10 percent of its total value. The model-determined transport through the FBC, stable throughout the entire simulation, agrees well with observation. It also includes a seasonal cycle of similar magnitude and phase (a minimum in February and a maximum in August). The model-determined  $\bar{T}$  and  $\bar{S}$  never reached a clear equilibrium state, however, and the mean values are about  $1.5$  °C and  $0.1$  psu higher than observed. The resulting  $\sigma_\theta$  is slightly lighter than observed (by  $0.03$  kg  $m^{-3}$ ), due to the opposite effects of  $T$  and  $S$  on density.

#### 4.2. Variation of the Model-Based NSOW at Mooring Arrays

[30] The time evolution of model-based ISOW at the SEI mooring array (not shown) is similar to that through the FBC. The model-determined transport ( $3.3 \pm 0.43$  Sv) also contains a seasonal variation, which is not seen in the mooring results by Saunders [1996]. The transport increase, when compared to  $2.2$  Sv through the FBC, is mainly due to entrained ambient water and IFR overflow water. Conse-

quently, the average temperature is increased to  $3.1 \pm 0.1$  °C. The average salinity is only slightly higher, however, because the modeled overflow source water (through the FBC) has high salinity similar to that of the entrained water.

[31] Further downstream over the Reykjanes Ridge and through the CGFZ, the time evolution of the model-determined transport and  $\bar{T}/\bar{S}$  are illustrated in Figure 15. The transport over the Reykjanes Ridge is highly variable during the first 5 years. It decreased about 1 Sv over the next 10 years, before leveling off in the final 5 years of the integration (Figure 15a). The decrease is largely due to the decreasing eastward flow from southern part of the CGFZ into the Iceland Basin. Through the CGFZ (Figure 15b), the model-based transport is stabilized after about 5 years of integration. The monthly transport values are more variable than upstream and a seasonal cycle no longer exists. Rather, the variation appears to be associated with the horizontal location and vertical extension of the eastward flow through the southern part of the CGFZ, somewhat similar to variations discussed by Saunders [1994] and Schott *et al.* [1999]. Both  $\bar{T}$  and  $\bar{S}$  exhibit a small trend that continues through the end of the 20 year simulation.

[32] At the ANG and SECF arrays in the western Irminger Sea, the time evolution of model-based transports and  $\bar{T}/\bar{S}$  are shown in Figure 16 for the two overflow layers. The transport evolution at the ANG array (Figure 16a) is similar to that of DSOW at the Denmark Strait, but without a clear seasonal variation. The downstream increase in transport is due to entrainment of ambient water as well as to contributions from the east (ISOW) and south (recirculation). As a result of the added transport,  $\bar{T}$  and  $\bar{S}$  rise significantly.

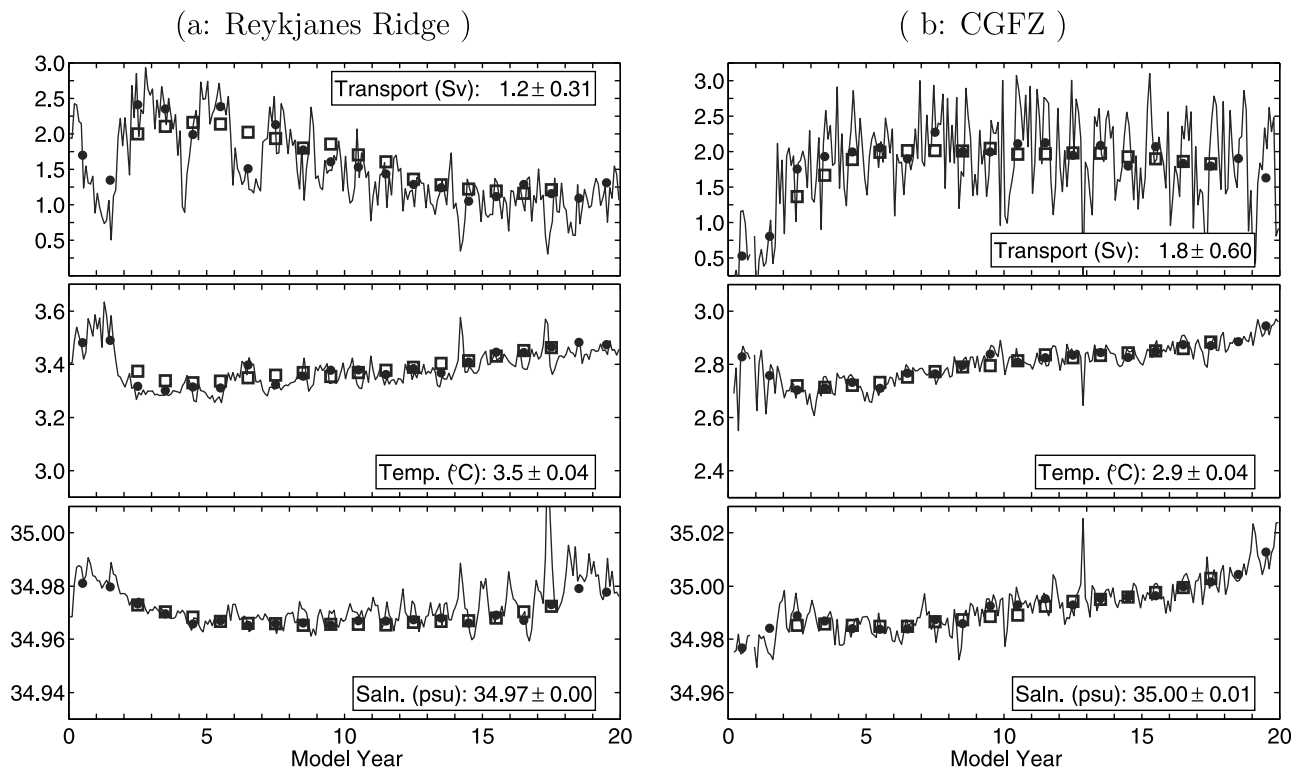


**Figure 15.** Time evolution of the model-based volume transport, average T and S of ISOW (a) over the Reykjanes Ridge and (b) through the northern channel of CGFZ. Lines, dots, and squares are results based on monthly means, annual means, and 5 year means, respectively.

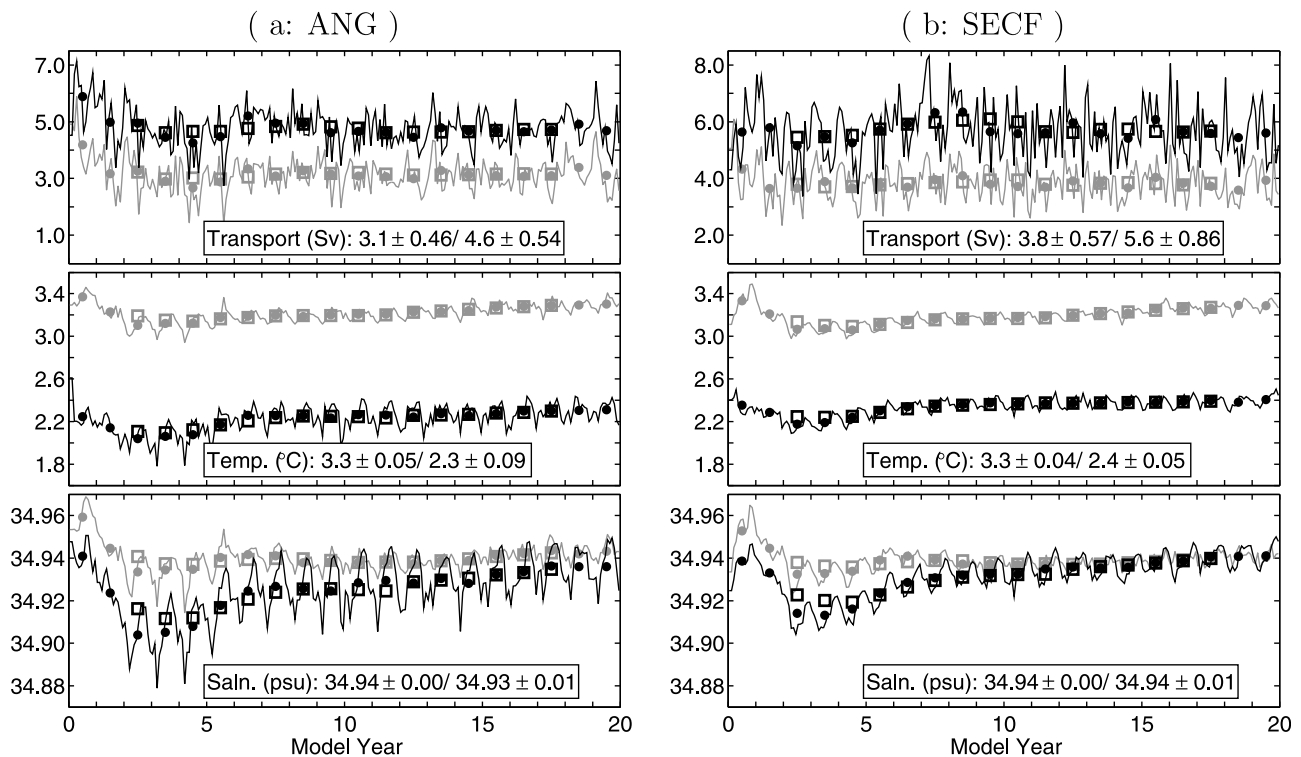


**Figure 16.** Time evolution of the model-based overflow characteristics at the (a) ANG and (b) SECF arrays in the western Irminger Sea. Gray and black colors denote overflow layers above and below 27.85 kg m<sup>-3</sup>. Lines, dots, and squares are results based on monthly means, annual means, and 5 year means, respectively.

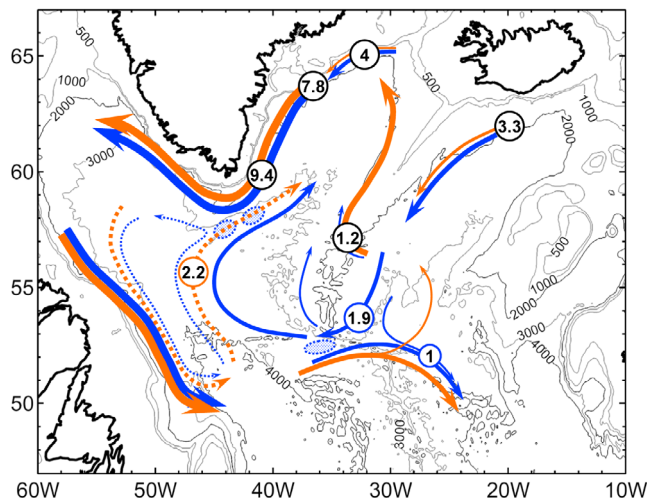


**Figure 17.** Model-based mean transport scheme for overflow water in the northern North Atlantic at  $\sigma_{\theta} \geq 27.85 \text{ kg m}^{-3}$  (blue) and  $27.80 \leq \sigma_{\theta} < 27.85 \text{ kg m}^{-3}$  (orange). The circled numbers are transports in Sv. Dashed arrows in the Labrador Sea denote large-scale recirculation. Patched ovals south of Cape Farewell and in the CGFZ denote small-scale recirculations and lateral mixing.

Further downstream at the SECF array (Figure 16b), the transport increases further, but  $\bar{T}$  and  $\bar{S}$  remains almost the same. This implies that the change of  $\bar{T}$  and  $\bar{S}$  for overflow in the western Irminger Sea is largely due to entrainment mixing, and that occurs primarily upstream of the ANG array.

## 5. Summary and Discussion

[33] Nordic Seas Overflow Water, specifically DSOW and ISOW, are key components of the North Atlantic Deep Water. Knowledge of the circulation and volume transports of the overflow water masses is therefore of fundamental importance in understanding the associated meridional overturning circulation of the Atlantic Ocean. In this study we have primarily considered the initial development phase of the overflow water, after it flows over the GIS Ridge but before it spreads into the subpolar gyre and beyond.

[34] Key elements of the observational database for overflow water transport in this region are acquired from five substantially instrumented, long-term moored current meter arrays. In considering the regional circulation as sampled by these arrays, there exists an unresolved question regarding the consistency/balance of these observed transports. Specifically, the transport of ISOW through CGFZ is too small, when compared to upstream at the SEI array and to downstream at the SECF array. To help address this question, we have used a basin-scale, eddy-resolving numerical simulation. The model results suggest that (1) in addition to the westward flow through the CGFZ, some ISOW flows westward into the Irminger Sea through gaps in the Reykjanes Ridge north of the CGFZ, and some ISOW flows southward into the Web along the eastern flank of the MAR south of the CGFZ and (2) in addition to the contributions of DSOW and ISOW from the north and east, the

overflow water transport at the SECF array includes some recirculation from the south.

[35] The general model-based circulation is summarized in Figure 17 and features that are pertinent to the specific questions, listed in section 1, are discussed below. Downstream of the SEI array in the Iceland Basin, flow of the model-based ISOW contains three main branches, or components, which are closely associated with bottom bathymetry (Figure 7). These branches eventually feed the different ISOW pathways: westward through gaps in the Reykjanes Ridge, westward through the northern channel of the CGFZ, and southward along the eastern flank of the MAR. In the southern part of the CGFZ, the model results suggest an eastward flow below  $27.80 \text{ kg m}^{-3}$ . Part of this eastward flow turns northward and flows into the Iceland Basin, while the rest turns southward and flows along the eastern flank of the MAR.

[36] West of the CGFZ, the model results indicate two flow pathways for the deep ISOW from the CGFZ into the Irminger Sea. Some ISOW turns northward immediately west of the CGFZ and flows along the western flank of the Reykjanes Ridge. The remaining flow follows a more complicated route to reach the area south of Cape Farewell (before flowing into the Irminger Sea). There the northeastward flowing deep ISOW and the southward flowing DWBC are adjacent and lateral interaction/mixing between them would be expected. A small amount of ISOW may join the DWBC without flowing into the Irminger Sea. Within the Irminger Sea, the deep ISOW with  $\sigma_{\theta}$  of  $27.85 \text{ kg m}^{-3}$  and larger merges with DSOW fairly uniformly (as a function of latitude). In contrast, more water in the layer of  $\sigma_{\theta}$  between  $27.80$  and  $27.85 \text{ kg m}^{-3}$  merges with DSOW north of the ANG array than south (Figure 10).

[37] The model results in addition depict recirculations in the overflow water (Figure 13). Below  $27.85 \text{ kg m}^{-3}$ , a large scale recirculation is present in the deepest part ( $>3500 \text{ m}$ ) of the Labrador Sea. Some small scale recirculations are also present in the area south and southeast of Cape Farewell and in the southern part of the CGFZ. Between  $27.80$  and  $27.85 \text{ kg m}^{-3}$ , a prominent component of the recirculation is depicted as an eastward to northeastward jet south of Cape Farewell that penetrates into the Irminger Sea. This model-based recirculation jet accounts for about 2.2 Sv out of the 9.4 Sv total transport for composite overflow water calculated through the SECF array.

[38] The results obtained from moored instrument arrays have provided a valuable benchmark for evaluating the performance of eddy-resolving, large-scale ocean models in simulating the downstream circulation of the overflow water source. The evaluation in this study includes detailed comparisons with observations along the mooring arrays, including the model-based mean volume transport, the vertical/lateral distribution of the water properties (especially salinity) associated with different water masses, as well as the velocity profiles of the overflow plume in the western Irminger Sea. These comparisons suggest that the model-based circulation is generally consistent with the available data. We have also investigated the temporal evolution of the model-based NSOW transports as well as T/S properties. While the T/S has some long-term trend, the transports are quite stable, especially in the final 5 years of the integration. Figures 14–16 suggest that a 1 year mean transport represents the long-

term mean well, probably in part due to the use of climatological forcing.

[39] There are, however, several aspects of the model results that need further improvement. The model-based ISOW through the CGFZ is slightly denser than observed and consequently flows at about 500 m deeper. This suggests that the diapycnal mixing in the model is too weak when the overflow water, after passing over the sill, descends along the northern and western slope of the Iceland Basin. This notion is similar to the experience with isopycnic model simulation of overflow water that is summarized in *Willebrand et al.* [2001], and an entrainment parameterization may be the key to improving the results. Another issue is that the modeled ISOW source in the FBC is warmer, more saline, and slightly less dense than observed. The exact reason is not clear. Diapycnal mixing and the T/S properties of MNAW and overflow source water in the Nordic Seas might be responsible. The model also does (does not) reproduce the observed bottom intensification of the overflow velocity profiles on the deep (shallow) part of continental slope in the western Irminger Sea. Increasing the vertical resolution does not improve this result. The transition of overflow water from pressure coordinates at the sill toward isopycnic layers along the slope might be important.

[40] Further numerical studies, with tools like passive tracers and/or numerical drifters to separate flows of different origins, would be helpful in better quantifying the circulation features described. We should also note that the simulation we have discussed does not simulate the northward flow of Antarctic Bottom Water (AABW). The model-based overflow water consequently misses the contribution from modified AABW, or Lower Deep Water [LDW, *McCartney* 1992], in the northern North Atlantic. As noted in section A3, LDW mixes with the ISOW that flows westward through the CGFZ and its (high silicate) signature is also present in the northern Irminger Sea. New experiments with improved representation of AABW/LDW are needed.

### Appendix A: Specific Comments on the Observational Base for Overflow Transports

[41] Appendix A is a detailed discussion of the database relevant to overflow transports in the western Irminger Sea and in the Iceland Basin, as listed in Table 1 in section 2.1. It also includes a comment concerning a possible influence on the ISOW characteristics in the Irminger Sea related to a contribution by Lower Deep Water (LDW) [*McCartney*, 1992]. The composite overflow water has been typically defined as having potential density ( $\sigma_\theta$ ) of  $27.80 \text{ kg m}^{-3}$  and larger. In the recent determinations and discussions of DSOW transports in the western Irminger Sea, *Dickson et al.* [2008] and *Bacon and Saunders* [2010] identify the boundary between DSOW and ISOW as having  $\sigma_\theta$  of  $27.85 \text{ kg m}^{-3}$ . As pointed out by these authors, the hydrographic data used in determining  $\sigma_\theta$  boundaries are typically acquired on setting, retrieval, and/or turn-around research cruises. As a result, the thickness (of overflow water) is less well determined in the mean than the velocity measured by using extensive long-term moored array data acquisition at dense temporal sampling intervals. We should also note that these

typically yearlong moored instrument arrays at different sites cover different periods over a total span of about two decades, and while a long-term trend in overflow transport has not clearly been detected, interannual variability has.

#### A1. Overflow Transports in the Western Irminger Sea

[42] Array 1 (in Figure 1) is colocated with the hydrographic “Transient Tracers in the Ocean” (TTO) section described by *Livingston et al.* [1985]. The salinity distribution along this TTO section has been used to identify different water masses in the Irminger Sea and a modified version is presented later in this discussion. The estimated composite overflow transport of 5.1 Sv is based on a moored instrument array with a record length of 368 days [*Dickson and Brown*, 1994]. They also found a similar value (5.2 Sv) 160 km upstream at Dohrn Bank, based on another moored instrument array of shorter duration. The transport of DSOW alone is not available at the TTO section, but Table 19.1 of *Dickson et al.* [2008] implies that it is close to that found at the ANG section.

[43] Array 2 is called the ANG array after its location offshore of Angmagssalik, Greenland. On their Figure 19.6, *Dickson et al.* [2008] have plotted the cross-sectional distribution of the mooring locations along with mean isopycnals of  $\sigma_\theta = 27.80$  and  $27.85 \text{ kg m}^{-3}$ . Most of their current meters are located between the  $27.85 \text{ kg m}^{-3}$  contour and the bottom, sampling the bottom-intensified flow associated with DSOW. Estimates of mean speeds in the regime of ISOW, identified with  $27.80 \leq \sigma_\theta < 27.85 \text{ kg m}^{-3}$ , are more sparsely located. The mean (downslope) current speeds for the period 1986 to 2005 are also listed in their Figure 19.6. Note that there is a large gap during 1990–1997, but these results nevertheless are very long and constitute a tremendous achievement in their acquisition. The estimates of transport (see their Table 19.2) through this ANG Array are 4 Sv for DSOW, and 7.3 Sv for the composite overflow. In their Table 19.1, *Dickson et al.* [2008] also estimated the interannual variability of DSOW transport. These estimates were based on a composite of three hydrographic sections shown in their Figure 19.10 (the center one being ANG). The transports varied from 2.5 to 5 Sv from 1997 through 2005, with an average of 3.6 Sv.

[44] Array 3 runs southeast of Cape Farewell, Greenland (here called SECF). In their Figure 2, *Bacon and Saunders* [2010] plotted a cross-sectional view of the mooring locations in relationship to the mean depth of the density surfaces ( $\sigma_\theta = 27.80$  and  $27.85 \text{ kg m}^{-3}$ ). Similar to the ANG array, most of the current meters were deployed at depths below  $\sigma_\theta$  of  $27.85 \text{ kg m}^{-3}$  for a similar reason (a focus on bottom-trapped currents). The roughly yearlong transports were found to be 4.5 Sv for DSOW, and 9 Sv for the composite overflow. The contribution of ISOW is therefore also about 4.5 Sv. For continuity, this 4.5 Sv of ISOW should arrive at the SECF section from the Iceland Basin, east of the Reykjanes Ridge. *Bacon and Saunders* [2010] also discussed the temporal variability of their records, and suggest that some interannual variability is present, but not dominant. Interannual variability in DSOW transport is also shown at the ANG array [*Dickson et al.*, 2008, Figure 19.7]

and at the Denmark Strait sill [Macrander *et al.*, 2005, Figure 2].

[45] A transport of 9 Sv for  $\sigma_\theta \geq 27.80 \text{ kg m}^{-3}$  at the SECF array is rather low in comparison with the previous estimate of 13.3 Sv across a section due south of Cape Farewell by Clarke [1984], as adopted by Dickson and Brown [1994]. The direct current measurements by Clarke [1984] include six current meters on three moorings for 60 days. So there could be a sampling issue in comparing this sparse data set with more substantially instrumented long-term direct measurements. The transport estimates by Clarke [1984] also involved CTD data taken along a section running south of Cape Farewell to Flemish Cap. The issue with respect to estimating the location of  $\sigma_\theta$  surfaces could also apply to Clarke's data set. The contour for  $\sigma_\theta = 27.80 \text{ kg m}^{-3}$  is about 800 m in the immediate vicinity of Cape Farewell in Figure 4c of Clarke [1984], compared to about 1400 m in Figure 2 of Bacon and Saunders [2010]. On his p.128, Clarke [1984] noted that his (transport) values are "useful estimates of the probable order of magnitudes of the transports of various currents and water types" as indicated by his data. Bacon and Saunders [2010] in their section 4.3 discussed the geostrophic reference level choices by Clarke [1984] in detail and concluded that the difference between 9 and 13 Sv (Bacon and Saunders actually suggest 13–16 Sv as a defensible range of values) could be due to temporal variability on interannual time scales.

[46] Our model results suggest the existence of considerations other than interannual variability for the differences in the overflow transports being considered. One possibility could be a change in the flow regime between south and southeast of Cape Farewell. Relative to the SECF section in the Irminger Sea, the overflows south of Cape Farewell involve a more pronounced presence of horizontal recirculations (on a variety of horizontal scales) from the Labrador Sea that could play a role in the transport difference. Within the Labrador Sea and close to the bottom, there may exist a large scale horizontal recirculation of overflow water [see Clarke, 1984, Figures 2 and 4]. This recirculation could also connect with the different overflow transports observed by Schott *et al.* [2004] east of the Grand Banks of Newfoundland and by Fischer *et al.* [2004] at the exit of the Labrador Sea. This speculation has not been suggested elsewhere as far as we know, but seems worthy of further examination.

## A2. Overflow Water in the Iceland Basin

[47] Array 4 (in Figure 1) is located southeast of Iceland (here called SEI). The estimate of the mean transport for ISOW is 3.2 Sv at  $\sigma_\theta \geq 27.80 \text{ kg m}^{-3}$ . Here Saunders [1996], his Figure 3 observed a well-defined bottom-trapped mean flow up on the western slope between the 1300 and 2200 m depth contours, while in contrast only a small mean flow is seen in the deep Iceland Basin. For comments on ISOW flowing into and within the deep Iceland Basin [see Hansen and Østerhus, 2000, Figures 43 and 49]. Saunders [1996] stated that the flow at the SEI array included only a very small contribution from over the IFR. However, Saunders [2001] changed the composition of the total flux of 3.2 Sv of ISOW to be 1.6 Sv of FBC overflow water, mixed with 0.8 Sv of entrained MNAW (7–8.5°C and

35.1–35.3 psu) and 0.8 Sv of Modified East Icelandic Water (MEIW, 1–3°C and 34.7–34.9 psu), and remarked that MEIW could only have come from over the IFR. A more detailed description of MEIW as an overflow water mass crossing the IFR may be found in the work of Hansen and Østerhus [2000, section 5.2].

[48] Array 5 was located along a north–south section across the CGFZ near 35°W. In his Figure 5, Saunders [1994] illustrates the distribution of mooring locations relative to the isopycnal depth of  $27.80 \text{ kg m}^{-3}$  ( $27.85 \text{ kg m}^{-3}$  is not shown), and to the salinity contour of 34.94 psu. The salinity distribution, also shown in his Figure 2, is the actual control used to identify ISOW. The estimated mean transport of 2.4 Sv is at  $S \geq 34.94$  psu but could be applied to  $\sigma_\theta \geq 27.80 \text{ kg m}^{-3}$  as well. The transport is dominated by temporal variability [Saunders, 1994, Figure 9]. The author speculated that the comparatively large amplitude overflow reversals observed might be connected to latitudinal migrations of the North Atlantic Current over the CGFZ, a speculation that was later found to be the case by subsequent observations [Schott *et al.*, 1999]. In an earlier study of deep flow within the CGFZ, Shor *et al.* [1980] found a cold freshwater type beneath ISOW with a flow tendency to the east, at least partially similar to the observations by Saunders [1994] and Schott *et al.* [1999].

[49] Hansen and Østerhus [2000] emphasized that a westward transport of 2.4 Sv in CGFZ seems too small for the total flow of ISOW over the GIS Ridge. It is also smaller than the 3.2 Sv observed at the upstream SEI section [Saunders, 1996]. The problem is augmented if flow through the CGFZ also contains a contribution from LDW. To reconcile this discrepancy, Hansen and Østerhus [2000] suggested a wide variety of possible ISOW paths in their Figure 54. One of these paths goes through a gap in the Reykjanes Ridge near 55°N to the north of the CGFZ. It turns out that the estimate for ISOW transport in the CGFZ by Shor *et al.* [1980] also yields 2.4 Sv to the west, seeming rather strong support for the surprisingly low transport found by Saunders [1994]. The size of the transport estimate by Shor *et al.* [1980] was not discussed by Saunders [1994] or Saunders [2001], probably due to the relatively limited long-term direct measurements involved.

[50] Interestingly, Shor *et al.* [1980] in their Figure 1 also suggest that some ISOW could leak westward through fracture valleys near 56.5°N into the Irminger Sea. Their premise was influenced by Vogt and Johnson [1973]. Based on a seismic reflection profile paralleling the axis of the Reykjanes Ridge, Vogt and Johnson [1973] suggested that the Reykjanes Ridge was broken by "many" transverse valleys between 52 and 57°N. They further pointed out that the asymmetry of the depositional sediments therein might imply that westward flow (of ISOW) crosses the Reykjanes Ridge. Over time, a few other authors in addition to Shor *et al.* [1980] and Hansen and Østerhus [2000] have questioned a 2.4 Sv transport of ISOW through the CGFZ and have noted it presents a conundrum because it is too small relative to observed transports of overflow water in the western Irminger Sea. Some of these other authors have suggested (but not demonstrated from either direct current measurements, nor tentatively illustrated by model results) a flow of ISOW through the gaps in the Reykjanes Ridge into the Irminger Sea.

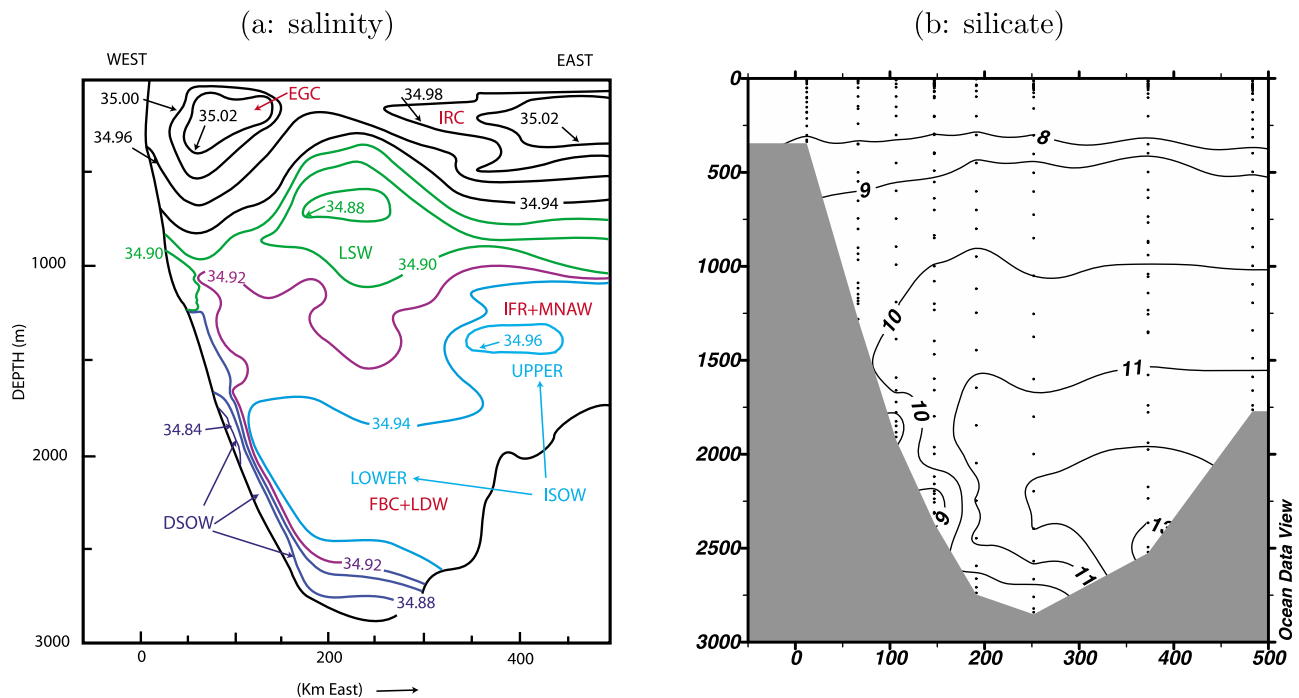


**Figure A1.** Vertical distributions of (a) salinity (in psu) and (b) silicate (in  $\mu\text{mol l}^{-1}$ ) along the hydrographic TTO section across the northern Irminger Sea (shown as blue dots in Figure 1). LSW (green contours) denotes Labrador Seawater, DSOW (dark blue contours) is Denmark Straits Overflow Water. ISOW (light blue contours) indicates the products associated with remote overflows (note upper and lower designations) across the Iceland-Scotland Ridge System that have made their way to the Irminger Sea. The red labels FBC, LDW, EGC, IRC, and MNAW indicate Faroe Bank Channel, Lower Deep Water, East Greenland Current, Irminger Current, and modified North Atlantic Water.

### A3. A Comment on an LDW Contribution

[51] *McCartney* [1992] suggested that modified Antarctic Bottom Water (AABW), or Lower Deep Water (LDW), penetrates into the northernmost part of the eastern North Atlantic Ocean, and mixes with the overflow transport measured along the western Irminger Sea. The presence of LDW in the Iceland Basin, identified with high silicate content, and the interaction with ISOW there were also discussed by *van Aken and de Boer* [1995] and *van Aken and Becker* [1996]. Because of LDW influence, the silicate content of the ISOW through the CGFZ ( $13\text{--}17\ \mu\text{mol l}^{-1}$ ) is significantly higher than that at the SEI array ( $9\text{--}10\ \mu\text{mol l}^{-1}$ ) [see *Saunders*, 1996, Figure 2d].

[52] In order to help identify a possible influence of LDW on the water masses in the Irminger Sea, the distributions of salinity and silicate along the TTO section are presented in Figure A1. The location of the section is shown as blue dots in Figure 1. The salinity plot was originally published by *Livingston et al.* [1985, Figure 2a] and was modified in *Dickson and Brown* [1994, Figure 3]. Here the salinity contours are colored with some added text indicating different water masses. The vertical stacking of DSOW, ISOW, LSW, as well as the saline MNAW in the upper level Irminger Current (IRC) and East Greenland Current (EGC) is relatively well known. Here we comment that the broad area of ISOW ( $S \geq 34.94$  psu) contains different levels of silicate (or tritium) [see *Livingston et al.*, 1985, Figure 2b]. The deep portion (of ISOW) is associated with a high silicate core of

$12\text{--}13\ \mu\text{mol l}^{-1}$ . The shallow portion that exists over the western slope of the Reykjanes Ridge between 1100 and 2000 m has a silicate content of  $10\text{--}11\ \mu\text{mol l}^{-1}$ . One possibility, consistent with our numerical results showing ISOW flowing over the Reykjanes Ridge, is that the shallow portion of the ISOW is perhaps composed of diluted IFR overflow water and entrained MNAW and that this water flows over the Reykjanes Ridge into the Irminger Sea without much LDW influence, while the deep portion of the ISOW is FBC water mixed with LDW that flows through the CGFZ before turning northward into the Irminger Sea.

[53] **Acknowledgments.** This work is a contribution to the project “U.S.-GODAE: Global Ocean Prediction using the HYbrid Coordinate Ocean Model (HYCOM)” funded under the National Ocean Partnership Program and to the 6.1 project “Global Remote Littoral Forcing via Deep Water Pathways” funded by the Office of Naval Research under program element 601153N. Simulations were performed on the supercomputer at the Naval Oceanographic Office, Stennis Space Center, MS, provided by the U.S. Defense Department High Performance Computing Modernization Program. The authors thank A. Wallcraft and E. J. Metzger from NRL/SSC for help on the configurations of numerical experiments. Figures 4a and A1b are plotted using *Ocean Data View* (<http://odv.awi.de>). This is Naval Research Laboratory publication number NRL/JA/7304-10-251, and it has been approved for public release.

### References

- Bacon, S. (1997), Circulation and fluxes in the North Atlantic between Greenland and Ireland, *J. Phys. Oceanogr.*, *27*, 1420–1435.  
 Bacon, S. (1998), Decadal variability in the outflow from the Nordic Seas to the deep Atlantic Ocean, *Nature*, *394*, 871–874.

- Bacon, S., and P. M. Saunders (2010), The deep western boundary current at Cape Farewell: Results from a moored current meter array, *J. Phys. Oceanogr.*, **40**, 815–829, doi:10.1175/2009JPO4091.1.
- Bianchi, G. G., and I. N. McCave (2000), Hydrography and sedimentation under the deep western boundary current on Björn and Gardar Drifts, Iceland basin, *Mar. Geol.*, **165**, 137–169.
- Bleck, R. (2002), An oceanic general circulation model framed in hybrid isopycnal-Cartesian coordinates, *Ocean Modell.*, **37**, 55–88.
- Carnes, M. R. (2009), Description and evaluation of GDEM-V 3.0, *Tech. Rep. 724/NRL/MR/7300-09-9165*, Nav. Res. Lab., Washington, D. C. (Available at <http://www7320.nrlssc.navy.mil/pubs/pubs.php>.)
- Chang, Y., Z. D. Garraffo, H. Peters, and T. Özgökmen (2009), Pathways of Nordic overflows from climate model scale and eddy resolving simulations, *Ocean Modell.*, **29**, 66–84.
- Chassignet, E. P., L. T. Smith, G. R. Halliwell, and R. Bleck (2003), North Atlantic simulations with the hybrid coordinate ocean model (HYCOM): Impact of the vertical coordinate choice, reference pressure, and thermobaricity, *J. Phys. Oceanogr.*, **33**, 2504–2526.
- Clarke, R. A. (1984), Transport through the Cape Farewell-Flemish Cap section, *Rapp. P. V. Reun. Cons. Int. Explor. Mer*, **185**, 120–130.
- Dickson, R. R., and J. Brown (1994), The production of North Atlantic Deep Water: Source, rates, and pathways, *J. Geophys. Res.*, **99**(C6), 12,319–12,341, doi:10.1029/94JC00530.
- Dickson, R. R., et al. (2008), The overflow flux west of Iceland: Variability, origins and forcing, in *Arctic-Subarctic Ocean Fluxes: Defining the Role of the Northern Seas in Climate*, edited by R. R. Dickson, J. Meincke, and P. Rhines, pp. 443–474, Springer, New York.
- Faure, V., and K. Speer (2005), Labrador Sea water circulation in the northern North Atlantic Ocean, *Deep Sea Res. Part II*, **52**, 565–581.
- Fischer, J., F. A. Schott, and M. Dengler (2004), Boundary circulation at the exit of the Labrador Sea, *J. Phys. Oceanogr.*, **34**, 1548–1570.
- Fleischmann, U., and M. Rhein (2000), The contribution of Iceland-Scotland overflow water to the formation of North East Atlantic deep water in the Iceland Basin and the West European Basin, *Int. WOCE Newsl.*, **38**, 20–26.
- Fleischmann, U., H. Hildebrandt, A. Putzka, and R. Bayer (2001), Transport of newly ventilated deep water from the Iceland Basin to the West European Basin, *Deep Sea Res. Part I*, **48**, 1793–1819.
- Girton, J. B., T. B. Sanford, and R. H. Käse (2001), Synoptic sections of the Denmark Strait Overflow, *Geophys. Res. Lett.*, **28**(8), 1619–1622, doi:10.1029/2000GL011970.
- Griffies, S. M., C. Böning, F. O. Bryan, E. P. Chassignet, R. Gerdes, H. Hasumi, A. Hirst, A.-M. Treguier, and D. Webb (2000), Developments in ocean climate modelling, *Ocean Modell.*, **2**, 123–192.
- Griffies, S. M., et al. (2009), Coordinated ocean-ice reference experiments (COREs), *Ocean Modell.*, **26**, 1–46.
- Hansen, B., and S. Østerhus (2000), North Atlantic-Nordic seas exchanges, *Prog. Oceanogr.*, **45**, 109–208.
- Hansen, B., and S. Østerhus (2007), Faroe Bank Channel overflow 1995–2005, *Prog. Oceanogr.*, **75**, 817–856.
- Hansen, B., S. Østerhus, W. R. Turrell, S. Jónsson, H. Valdimarsson, H. Hátún, and S. M. Olsen (2008), The inflow of Atlantic water, heat, and salt to the Nordic Seas across the Greenland-Scotland Ridge, in *Arctic-Subarctic Ocean Fluxes: Defining the Role of the Northern Seas in Climate*, edited by R. R. Dickson, J. Meincke, and P. Rhines, pp. 15–43, Springer, New York.
- Holliday, N. P., S. Bacon, J. Allen, and E. L. McDonagh (2009), Circulation and transport in the Western Boundary Currents at Cape Farewell, Greenland, *J. Phys. Oceanogr.*, **39**, 1854–1870.
- Kara, A. B., H. E. Hurlburt, and A. J. Wallcraft (2005), Stability-dependent exchange coefficients for air-sea fluxes, *J. Atmos. Oceanic Technol.*, **22**, 1080–1094.
- Käse, R. H., J. B. Girton, and T. B. Sanford (2003), Structure and variability of the Denmark Strait overflow: Model and observations, *J. Geophys. Res.*, **108**(C6), 3181, doi:10.1029/2002JC001548.
- Kieke, D., and M. Rhein (2006), Variability of the overflow water transport in the western subpolar North Atlantic, 1950–97, *J. Phys. Oceanogr.*, **36**, 435–456, doi:10.1175/JPO2847.1.
- Large, W. G., J. C. McWilliams, and S. C. Doney (1994), Ocean vertical mixing: A review and a model with a nonlocal boundary layer parameterization, *Rev. Geophys.*, **32**(4), 363–403.
- Lavender, K. L., R. E. Davis, and W. B. Owens (2000), Mid-depth recirculation observed in the interior Labrador and Irminger Seas by direct velocity measurements, *Nature*, **407**, 66–69.
- Lavender, K. L., W. B. Owens, and R. E. Davis (2005), The middepth recirculation of the subpolar North Atlantic Ocean as measured by subsurface floats, *Deep Sea Res. Part I*, **52**, 767–785.
- Legg, S., et al. (2009), Improving oceanic overflow representation in climate models: The Gravity Current Entrainment Climate Process Team, *Bull. Am. Meteorol. Soc.*, **90**, 657–670, doi:10.1175/2008BAMS2667.1.
- Lherminier, P., H. Mercier, C. Gourcuff, M. Álvarez, S. Bacon, and C. Kermabon (2007), Transports across the 2002 Greenland-Portugal Ovide section and comparison with 1997, *J. Geophys. Res.*, **112**, C07003, doi:10.1029/2006JC003716.
- Livingston, H. D., J. H. Swift, and H. G. Ostlund (1985), Artificial radio-iodide tracer supply to the Denmark Strait Overflow between 1972 and 1981, *J. Geophys. Res.*, **90**(C4), 6971–6982, doi:10.1029/JC090iC04p06971.
- Macrander, A., U. Send, H. Valdimarsson, S. Jónsson, and R. H. Käse (2005), Interannual changes in the overflow from the Nordic Seas into the Atlantic Ocean through Denmark Strait, *Geophys. Res. Lett.*, **32**, L06606, doi:10.1029/2004GL021463.
- Mauritzen, C. (1996a), Production of dense overflow waters feeding the North Atlantic across the Greenland-Scotland Ridge: Part 1. Evidence for a revised circulation scheme, *Deep Sea Res. Part I*, **43**, 769–806.
- Mauritzen, C. (1996b), Production of dense overflow waters feeding the North Atlantic across the Greenland-Scotland Ridge: Part 2. An inverse model, *Deep Sea Res. Part I*, **43**, 807–835.
- McCartney, M. S. (1992), Recirculating components to the deep boundary current of the northern North Atlantic, *Prog. Oceanogr.*, **29**, 283–383.
- McCartney, M. S., and C. Mauritzen (2001), On the origin of the warm inflow to the Nordic Seas, *Prog. Oceanogr.*, **51**, 125–214.
- Østerhus, S., T. Sherwin, D. Quadfasel, and B. Hansen (2008), The overflow transport east of Iceland, in *Arctic-Subarctic Ocean Fluxes: Defining the Role of the Northern Seas in Climate*, edited by R. R. Dickson, J. Meincke, and P. Rhines, pp. 443–474, Springer, New York.
- Riemenschneider, U., and S. Legg (2007), Regional simulations of the Faroe Bank Channel overflow in a level model, *Ocean Modell.*, **17**, 93–122.
- Ross, C. K. (1984), Temperature-salinity characteristics of the overflow water in Denmark Strait during OVERFLOW 73', *Rapp. P. V. Reun. Cons. Int. Explor. Mer*, **185**, 111–119.
- Rudels, B., P. Eriksson, H. Grönvall, R. Hietala, and J. Launiainen (1999), Hydrographic observations in Denmark Strait in fall 1997, and their implications for the entrainment into the overflow plume, *Geophys. Res. Lett.*, **26**(9), 1325–1328, doi:10.1029/1999GL900212.
- Sarafanov, A., A. Falina, H. Mercier, P. Lherminier, and A. Sokov (2009), Recent changes in the Greenland-Scotland overflow derived water transport inferred from hydrographic observations in the southern Irminger Sea, *Geophys. Res. Lett.*, **36**, L13606, doi:10.1029/2009GL038385.
- Saunders, P. M. (1994), The flux of overflow water through the Charlie-Gibbs fracture zone, *J. Geophys. Res.*, **99**(C6), 12,343–12,355, doi:10.1029/94JC00527.
- Saunders, P. M. (1996), The flux of dense cold water overflow southeast of Iceland, *J. Phys. Oceanogr.*, **26**, 85–95.
- Saunders, P. M. (2001), The dense northern overflows, in *Ocean Circulation and Climate*, edited by G. Siedler, J. Church, and J. Gould, pp. 401–417, Academic, New York.
- Schott, F., L. Stramma, and J. Fischer (1999), Interaction of the North Atlantic current with deep Charlie-Gibbs fracture zone throughflow, *Geophys. Res. Lett.*, **26**(3), 364–372, doi:10.1029/1998GL900223.
- Schott, F., L. Stramma, R. Zantopp, M. Dengler, J. Fischer, and M. Wibaux (2004), Circulation and deep water export at the western exit of the sub-polar North Atlantic, *J. Phys. Oceanogr.*, **34**, 817–843.
- Shi, X., L. P. Roed, and B. Hackett (2001), Variability of the Denmark Strait overflow: A numerical study, *J. Geophys. Res.*, **106**(C10), 22,277–22,294, doi:10.1029/2000JC000642.
- Shor, A., P. Lonsdale, C. D. Hollister, and D. Spencer (1980), Charlie-Gibbs fracture zone: Bottom-water transport and its geological effects, *Deep Sea Res. Part A*, **27**, 325–345.
- Smith, W. H. F., and D. T. Sandwell (1997), Global seafloor topography from satellite altimetry and ship depth soundings, *Science*, **277**, 1957–1962.
- Uppala, S. M., et al. (2005), The ERA-40 re-analysis, *Q. J. R. Meteorol. Soc.*, **131**, 2961–3012, doi:10.1256/qj.04.176.
- van Aken, H. M., and G. Becker (1996), Hydrography and throughflow in the north-eastern North Atlantic Ocean: The NASEN project, *Prog. Oceanogr.*, **38**, 297–346.
- van Aken, H. M., and C. J. de Boer (1995), On the synoptic hydrography of intermediate and deep water masses in the Iceland Basin, *Deep Sea Res. Part I*, **42**, 165–189.
- Vogt, P. R., and G. L. Johnson (1973), A longitudinal seismic reflection profile of the Reykjanes Ridge: Part 1. Evidence for west-flowing bottom water, *Earth Planet. Sci. Lett.*, **18**, 45–48.
- Willebrand, J., B. Barnier, C. Böning, C. Dieterich, P. D. Killworth, C. L. Provost, Y. Jia, J. Molines, and A. L. New (2001), Circulation characteristics in three eddy-permitting models of the North Atlantic, *Prog. Oceanogr.*, **48**, 123–161.
- Worthington, L. V., and W. R. Wright (1970), *North Atlantic Ocean Atlas of Potential Temperature and Salinity in the Deep Water Including Tem-*

*perature, Salinity and Oxygen Profiles From the Erika Dan Cruise of 1962*, vol. II, Woods Hole Oceanogr. Inst., Woods Hole, Mass.

---

E. P. Chassignet, Center for Ocean-Atmospheric Prediction Studies, Florida State University, 2035 E. Paul Dirac Dr., 200 RM Johnson Bldg., Tallahassee, FL 32306-2840, USA.

P. J. Hogan and H. E. Hurlburt, Oceanography Division, Naval Research Laboratory, Building 1009, Stennis Space Center, MS 39529, USA.

W. J. Schmitz Jr., Harte Research Institute, Texas A&M University, 6300 Ocean Dr., Corpus Christi, TX 78412-5869, USA.

X. Xu, Department of Marine Science, University of Southern Mississippi, 1020 Balch Blvd., Stennis Space Center, MS 39529, USA. (xiaobiao.xu@usm.edu)